Dye laser excitation studies of the Ã2Π(100)/(020)–X̃2Σ+(020)/(000) bands of CaOD: Analysis of the Ã2Π(100)(020) Fermi resonance

Mingguang Li and John A. Coxon

Citation: The Journal of Chemical Physics **104**, 4961 (1996); doi: 10.1063/1.471762
View online: http://dx.doi.org/10.1063/1.471762
View Table of Contents: http://scitation.aip.org/content/aip/journal/jcp/104/13?ver=pdfcov
Published by the AIP Publishing

Dye laser excitation studies of the $\tilde{A}\,^2\Pi(100)/(020)-\tilde{X}\,^2\Sigma^+(020)/(000)$ bands of CaOD: Analysis of the $\tilde{A}\,^2\Pi(100)\sim(020)$ Fermi resonance

Mingguang Li and John A. Coxon
Department of Chemistry, Dalhousie University, Halifax, Nova Scotia, B3H 4J3 Canada

(Received 17 October 1995; accepted 18 December 1995)

The CaOD $\tilde{A}\,^2\Pi(100)/(020)-\tilde{X}\,^2\Sigma^+(020)/(000)$ bands have been rotationally analyzed via high resolution laser excitation. All measured line positions have been included in a global matrix deperturbation that takes account of the Renner–Teller, spin–orbit, and Fermi resonance interactions occurring in the $\tilde{A}(100)(020)\,^2\Pi$ vibronic manifold. The corresponding bands of CaOH were studied previously; in the present work, two new CaOH subbands, $\tilde{A}(020)\kappa\,^2\Pi-\tilde{X}(020)$, were recorded, and the complete data set for CaOH has been refitted using the improved model reported in this paper. The Fermi resonance parameter for CaOD has been determined as $|W_1|=5.2707(22)$ cm^{-1}; for CaOH, the newly determined value, $|W_1|=10.3256(5)$ cm^{-1} is very close to that determined originally. The (100)~(020) Fermi interaction in the $\tilde{X}\,^2\Sigma^+$ state has also been investigated for both isotopomers. The vibrational dependence of the Renner–Teller parameter $\epsilon\omega_2$ has been characterized, yielding values of the anharmonic quartic parameter, $\hat{g}_4=-0.1002(3)$ and $-0.0666(5)$ cm^{-1} for CaOH and CaOD, respectively. The ''harmonic'' Renner–Teller parameters are thus deduced as $\epsilon\omega_2=-35.6622(19)$ and $-26.5605(31)$ cm^{-1} for CaOH and CaOD, respectively. The equilibrium bond lengths, molecular force constants and Coriolis coupling constants for both the $\tilde{A}$ and $\tilde{X}$ states have been evaluated. © *1996 American Institute of Physics.* [S0021-9606(96)00512-8]

I. INTRODUCTION

The electronic spectra of alkaline earth monohydroxides are complex owing to overlapping of bands and interactions between the electronic and nuclear degrees of freedom. For CaOH and CaOD, analysis of the vibrational levels with $v_1\geqslant 1$ and $v_2\geqslant 2$ is further complicated by Fermi resonance interactions that arise from near degeneracies due to $\omega_1\approx 2\omega_2$. On the other hand, however, valuable information on the cubic anharmonic force field can be obtained if such interactions can be analyzed. CaOH has been an excellent candidate for studying such interactions since it is readily produced in the laboratory and its low-lying electronic states are located in a convenient region for dye laser excitation. As previously described,[1,2] the use of a Broida oven[3] as the molecular source has greatly reduced the spectral density, compared with the flames. It has also been demonstrated[4–6] that selective detection of laser induced fluorescence is very effective for simplifying excitation spectra and enhancing signal/noise ratio.

The (100)~(020) Fermi resonance in the $\tilde{A}\,^2\Pi$ electronic state of CaOH was investigated previously by the present authors.[5] The $\tilde{A}(020)$ level is approximately 73 cm^{-1} above the $\tilde{A}(100)$ level. At first sight, it would appear that these levels are sufficiently far apart that no significant interaction would occur. However, the spin–orbit and vibronic splittings bring the $\tilde{A}(020)\mu\,^2\Pi_{3/2}$ component to near coincidence with the $\tilde{A}(100)\,^2\Pi_{3/2}$ component, as depicted in Fig. 1(a). Very strong Fermi resonance was observed and analyzed. The present publication reports the investigation of the corresponding system of CaOD. In the CaOD $\tilde{A}\,^2\Pi$ state, the (020) level is approximately 85 cm^{-1} below the (100) level, as shown in Fig. 1(b). Again, the spin–orbit and vibronic splittings lead to a near degeneracy, in this case between the $(100)\,^2\Pi_{1/2}$ and $(020)\kappa\,^2\Pi_{3/2}$ components. The strongest interaction occurs between these two components, and since it originates from the operators H(Fermi resonance)$\times H$(S-uncoupling), as will be shown later in Sec. IV, the interaction is J dependent. This situation has made the analysis and modeling even more difficult than that in CaOH, for which the strongest interaction involves only the Fermi resonance matrix element, and hence is J independent.

The spectroscopic study of two isotopic species provides more benefit than a simple doubling of the data. In the $\tilde{A}(100)/(020)$ vibronic manifolds of CaOH and CaOD, the Renner–Teller, spin–orbit, and Fermi resonance interactions occur simultaneously, and pose a great challenge to spectral analysis and model fitting. The similarity and difference between the spectra of the isotopic species provide valuable diagnostic information. The isotope relation of the molecular constants determined from experimental data is an excellent criterion for assessment of the quality of the data set and deperturbation models. Although such relation holds strictly only for the constants obtained at equilibrium configuration, the molecular constants for the (100) and (020) levels of CaOH/CaOD obtained in this work still obey the isotope relation very well. This situation not only confirms the quality of the data sets and the deperturbation model but also provides a rare experimental example that the isotope relations still hold very well at low excited vibrational levels in a radical with a linear structure.

Previously, we have performed detailed analyses of the (010) levels in the $\tilde{A}$ and $\tilde{X}$ states for both CaOH and CaOD.[6] The analysis of the (100) and (020) levels for both isotopomers have now been completed. The well determined

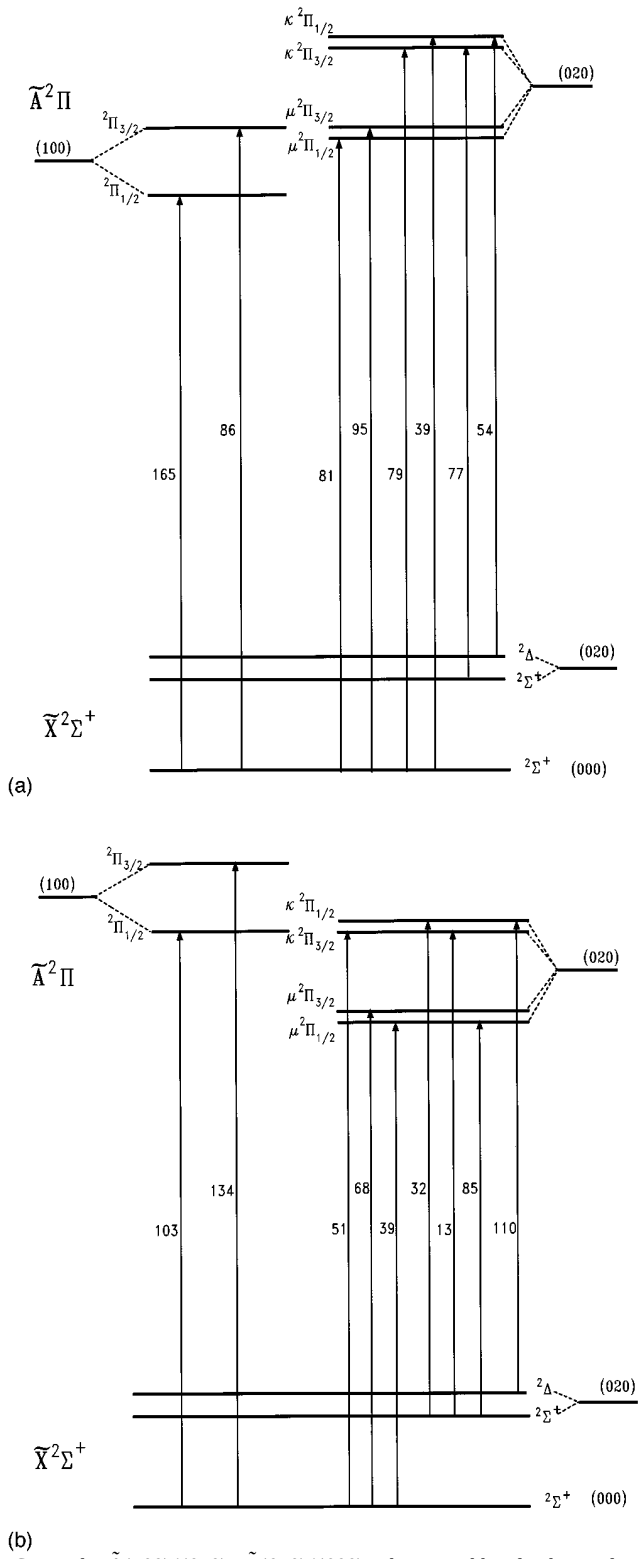

FIG. 1. The $\tilde{A}(100)/(020)-\tilde{X}(020)/(000)$ vibronic subbands observed via laser excitation: (a) for CaOH, (b) for CaOD. Each number attached to a vertical line indicates the number of rotational transitions observed for the corresponding subband.

vibration–rotation interaction parameters α_2 and Fermi resonance parameters W_1 now provide sufficient information for determining some of the cubic anharmonic force constants. It becomes possible to evaluate the equilibrium bond lengths and force field with good accuracy for the $\tilde{A}$ state as well as for the $\tilde{X}$ state. Unfortunately, the excited O–H stretching levels have still not been observed despite much effort in this and other laboratories. However, since a good approximation can be made for the O–H stretch mode, the lack of experimental information has little effect on the calculated quantities; this will be discussed later in this paper.

The $\tilde{A}(100)-\tilde{X}(000)$ band of CaOD was observed previously in this laboratory.[7] However, owing to the strong Fermi resonance encountered in the upper state, this band was not characterized satisfactorily. In the present work, this band was reinvestigated along with the $\tilde{A}(020)-\tilde{X}(020)/(000)$ bands. In order to maintain high precision of the data set, all the rotational lines that were recorded previously with significant broadening due to the unresolved spin–rotation splittings in the lower state have been omitted from the present data set. Two new branches in the $\tilde{A}(100)-\tilde{X}(000)$ band, $^SR_{21}$ and $^OP_{12}$, which are not affected by the spin–rotation splittings, have been recorded to high J in the present work. The strong $Q_1+{}^QR_{12}$ branches in the range $J'=30\frac{1}{2}-40\frac{1}{2}$ have been resolved and measured in this work using a computer program for measuring overlapped lines consisting of two or more Gaussian profiles.

During the investigation of CaOD in the present work, two more subbands for CaOH were also recorded. The previous study[5] of the CaOH $\tilde{A}(020)$ level only involved transitions excited from the $\tilde{X}(000)$ level. The $\tilde{A}(020)\kappa\,^2\Pi_{1/2}$ vibronic component of CaOH was not well characterized owing to the extremely small transition strength between the $\tilde{X}(000)\ ^2\Sigma^+$ level and the $\tilde{A}(020)\kappa\,^2\Pi_{1/2}$ level. The hot band excitation from the $\tilde{X}(020)$ levels to the $\tilde{A}(020)\kappa\,^2\Pi$ levels conducted in the present work provides much new information for both the $\tilde{A}(020)$ and $\tilde{X}(020)$ levels of CaOH. In addition, it was found that an l-type doubling matrix element was missing in the original matrix[5,8] constructed for the $\tilde{A}(100)/(020)$ vibronic states. Significant modifications of the effective Hamiltonian matrix for this vibronic manifold have been made in the present work, as described later in Sec. IV. It was necessary, therefore, to refit the entire data set for CaOH. The new results for CaOH, as well as the results for CaOD, will be presented in this publication.

II. FERMI RESONANCE

Like the vibration–rotation interaction, the Fermi resonance interaction is a manifestation of the cubic anharmonic force field. One of the force constants, ϕ_{122} or ϕ_{322}, in the dimensionless normal coordinates can be directly calculated from the Fermi resonance parameters. Following Fermi's recognition[9] of this phenomenon in CO_2, most subsequent work has been performed for nondegenerate electronic states (Σ states). Hougen,[10] however, carried out a quantum mechanical treatment of Fermi resonance of the $(v_1+1,v_2,v_3)\sim(v_1,v_2+2,v_3)$ type in linear triatomic Π electronic states, which are also subject to the Renner–Teller effect. He introduced two Fermi resonance parameters, W_1 and W_2, for the Π electronic state, replacing the single parameter W for a Σ state. These two parameters are defined as

$$W_1=\tfrac{1}{2}(k'_{122}+k''_{122})(\hbar/4\pi c\omega_2)(\hbar/4\pi c\omega_1)^{1/2}, \quad (1)$$

$$W_2=\tfrac{1}{2}(k'_{122}-k''_{122})(\hbar/4\pi c\omega_2)(\hbar/4\pi c\omega_1)^{1/2}, \quad (2)$$

where ω_1 and ω_2 are harmonic vibrational frequencies, and k_{122} is a cubic anharmonic force constant in the normal coordinate expansion of the potential. The single and double primes refer to the two component electronic wave functions which are symmetric and antisymmetric, respectively, with respect to reflection in the plane of the bent molecule. As implied by Eq. (2), W_2 depends on the magnitude of the vibronic interaction that leads to splitting of the potential. Hougen's derivation[10] of the Fermi resonance matrix elements for a $^2\Pi$ electronic state used vibronic wave functions obtained from a first-order perturbation treatment of the Renner–Teller and spin–orbit effects, which are both assumed to be small compared to the bending frequency. The corresponding matrix elements employed in this work are the same as those in Ref. 8 derived according to Ref. 10.

In the $\tilde{A}\ ^2\Pi$ electronic state, the vibrational level (100) is split into two components, $^2\Pi_{1/2}$ and $^2\Pi_{3/2}$, and (020) into six components, $\mu\ ^2\Pi_{1/2}$, $\mu\ ^2\Pi_{3/2}$, $\kappa\ ^2\Pi_{1/2}$, $\kappa\ ^2\Pi_{3/2}$, $^2\Phi_{5/2}$, and $^2\Phi_{7/2}$ by spin–orbit and vibronic interactions. The (100) $^2\Pi$ manifold and the (020) $^2\Pi$ manifold are the same symmetry species and lie close in energy, leading to strong Fermi resonance. It is advantageous and, actually, necessary to study the two manifolds simultaneously. The $^2\Phi$ components do not interact significantly with any $^2\Pi$ components, and were not considered in this work. Figure 1(a) shows schematically the subbands for CaOH observed mostly in our previous work; Fig. 1(b) shows the subbands for CaOD observed in the present work. Each number attached to a vertical line indicates the number of rotational transitions observed for the corresponding subband.

III. EXPERIMENTAL DETAILS

The experimental set up in this work is the same as described in our previous publications.[5,6] Briefly, the gas phase CaOD radicals were produced in a Broida oven by the reaction of Ca vapor with a flow of D_2O that had been passed through a microwave discharge (2450 MHz). The $Ca+D_2O$ reaction is endothermic and microwave discharge was essential for CaOD production, which was associated with strong orange color chemiluminescence. Similar chemiluminescence is observed in the production of CaOH using the exothermic $Ca+H_2O_2$ reaction. The mechanism by which a discharge promotes the $Ca+D_2O$ reaction is not understood; one possibility is the formation of vibrationally excited D_2O; vibrational excitation in a reactant is known to promote endothermic reactions[11,12] very effectively. When the microwave discharge was initiated using a Tesla coil, problems from damage to the electronics of the dye laser system were encountered. Fortunately, it was found that the microwave discharge could be induced without the use of the Tesla coil by carefully adjusting the total pressure in the reaction chamber to about 2 Torr.

A Coherent 699-29 ring dye laser was operated in single mode with Rhodamin 6G dye for the $\tilde{A}(100)/(020)-\tilde{X}(000)$ bands and Sulforhodamin B dye for the $\tilde{A}(020)-\tilde{X}(020)$ band. The laser induced fluorescence (LIF) was imaged onto the entrance slit of a 1.26 m Spex monochromator which functions as a tunable band-pass filter for selective detection of the LIF. The slit width of the monochromator was set typically at 1 mm, corresponding to a spectral width of ~3.5 Å. When $\Delta v_1=+1$ or $\Delta v_2=+2$ transitions were excited, $\Delta v_i=0$ emissions were the dominant (>90%) component of the LIF. By maintaining the monochromator at a frequency that was lower than the scanning laser frequency by an amount corresponding to the vibrational interval, the $\Delta v_i=0$ component of the LIF was selectively detected.

Rotational line positions of the excitation spectra were measured using the 699-29 internal wave meter. An I_2 excitation spectrum was recorded simultaneously and compared to the standard I_2 atlas[13] to calibrate the wave meter measurements. The average measurement accuracy was estimated to be 0.0035 cm^{-1}.

IV. LIF EXCITATION AND DISPERSION

Both $\tilde{A}(100)-\tilde{X}(000)$ and $\tilde{A}(020)-\tilde{X}(000)$ transitions are allowed by dipole selection rules. However, owing to the unfavorable Franck–Condon factors, the (100)–(000) band is approximately ten times weaker than the (000)–(000) band, while the (020)–(000) band is again ~10 times weaker than the (100)–(000) band. Although strong Fermi resonance between (100) and (020) tends to mix these two vibrational levels and even the transition strengths between the two bands, excitations to the (020)$\kappa\ ^2\Pi_{1/2}$ vibronic level from $\tilde{X}(000)$ are still extremely weak, and the present work relied mainly on the use of hot band excitations from $\tilde{X}(020)$. This is probably associated with the small Fermi interaction matrix element between (020)$\kappa\ ^2\Pi_{1/2}$ and (100) $^2\Pi_{1/2}$, as shown later in Table I ($W_2\approx 0$).

Although $\Delta v_i=0$ hot band excitations to the $\tilde{A}(100)/(020)$ levels would have the largest Franck–Condon factors, a majority of the CaOD excitation spectra were taken from the $\tilde{X}(000)$ level, which was also the case for CaOH. This approach has several advantages. First, the $\tilde{X}(000)$ level has much larger population than the excited (100) or (020) levels in the Broida oven. Second, these bands are located in a region that is much less congested than the $\Delta v_i=0$ bands. Third, it is more convenient for the use of the selective LIF detection, which not only simplifies the spectra and improves the signal/noise ratio, but also provides considerable diagnostic information.

For CaOD, the $\tilde{A}(100)/(020)-\tilde{X}(000)$ bands span a range of 16 470–16 715 cm^{-1}. The excitation spectra were recorded twice in the entire region, first using selective LIF detection with a frequency difference $\Delta\bar{\nu}=605$ cm^{-1} ($\approx\omega_1$), and then with $\Delta\bar{\nu}=519$ cm^{-1} ($\approx 2\omega_2$). In the lower-frequency region, 16 470–16 530 cm^{-1}, only the $\Delta\bar{\nu}=519$ cm^{-1} spectrum exhibits clear structure, which was identified as the $\tilde{A}(020)\mu\ ^2\Pi_{1/2,3/2}-\tilde{X}(000)\ ^2\Sigma^+$ subbands. Although these subbands are quite weak, the R_2, Q_2, and P_1 branches have fair intensities. The rotational lines of these branches did not become noticeably broader even at high J ($=40\frac{1}{2}$),

indicating that the satellite lines are very weak and the upper state conforms to Hund's case (b). In the high-frequency region, 16 615–16 715 cm^{-1}, the $\Delta\bar{\nu}=605$ cm^{-1} spectrum has the highest intensity among all subbands observed for CaOD in this work, while no spectrum was detectable with $\Delta\bar{\nu}=519$ cm^{-1}. The $\Delta\bar{\nu}=605$ cm^{-1} spectrum in this region was readily assigned as the $\tilde{A}(100)\ ^2\Pi_{3/2}-\tilde{X}(000)$ subband, which showed a typical structure for a case (a) $^2\Pi-^2\Sigma^+$ transition. In these two regions the selective detection has given information that leads to direct identification of the vibronic species involved, and only several resolved fluorescence spectra were required for J and e/f assignment. In a narrow region, 16 560–16 600 cm^{-1}, the spectra recorded with $\Delta\bar{\nu}=605$ and $\Delta\bar{\nu}=519$ cm^{-1} showed basically the same structure and intensity, and were very congested and complex. It appeared that two subbands are excited in this region. One of then must correspond to the $\tilde{A}(100)\ ^2\Pi_{1/2}$ component; the other was likely to be associated with the $\tilde{A}(020)\kappa\ ^2\Pi_{3/2}$ component because the $\tilde{A}(020)\kappa\ ^2\Pi_{1/2}$ component should not be so close to $\tilde{A}(100)\ ^2\Pi_{1/2}$ owing to the expected strong repulsion between the two components by Fermi resonance. However, the $\tilde{A}(020)\kappa\ ^2\Pi_{1/2}-\tilde{X}(000)$ subband could not be observed elsewhere with either $\Delta\bar{\nu}=519$ cm^{-1} or $\Delta\bar{\nu}=605$ cm^{-1} scan. Numerous resolved fluorescence spectra were recorded for vibronic and rotational assignment. The final assignment of the vibronic species was not made until the hot band $\tilde{A}(020)\kappa\ ^2\Pi_{1/2}-\tilde{X}(020)$ was observed and analyzed. This hot band was heavily blended by other $\Delta v_i=0$ bands. Another type of selective detection method was then employed, namely, scanning the R branch and detecting the corresponding P branch, or *vice versa*. Such a method requires some preliminary knowledge of the rotational structure for both upper and lower states. Since the rotational constants of the $\tilde{X}(02^00)$ and (02^20) levels were determined previously through resolved fluorescence,[14] though with relatively large uncertainty, this band was finally recorded with good signal/noise ratio after several trial scans.

In the case of CaOH, the $\tilde{A}(020)\kappa\ ^2\Pi_{1/2}-\tilde{X}(000)$ subband was observed in our previous work,[5] but was very weak and not well characterized. The hot band $\tilde{A}(020)\kappa\ ^2\Pi-\tilde{X}(020)$ for CaOH was recorded in the present work in order to better characterize the $\kappa\ ^2\Pi$ state. Such hot band excitations also served for more accurate characterization of the $\tilde{X}(020)$ level for both CaOD and CaOH.

Figure 2 shows two nearby band heads in the excitation spectrum of CaOD, recorded using selective detection with $\Delta\bar{\nu}=519$ cm^{-1}. The band head at the lower frequency side was identified as formed by the $\tilde{A}(020)\kappa\ ^2\Pi_{3/2}-\tilde{X}(000)\ ^2\Sigma^+\ P_1$ branch, and the $\kappa\ ^2\Pi_{3/2}$ vibronic state was assigned as the F_1 component owing to the negative effective spin–orbit coupling. The other head was assigned to the $\tilde{A}(100)\ ^2\Pi_{1/2}-\tilde{X}(000)\ ^2\Sigma^+\ P_1$ branch. When the frequency difference was set at 605 cm^{-1}, the excitation spectrum in the same region appeared essentially the same as the one in Fig. 2. This observation is in accord with the heavy mixing of the two upper states; they actually exchange leading characters at $J'\geqslant 41\frac{1}{2}$.

Although the spectrum analysis was greatly facilitated

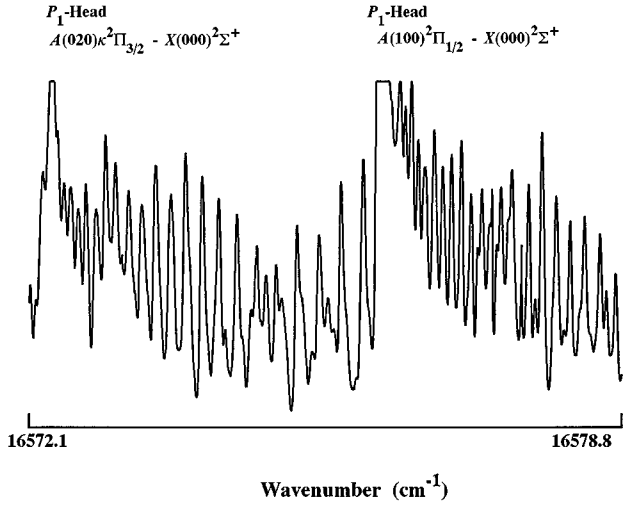

FIG. 2. A portion of the excitation spectrum of CaOD, recorded using selective LIF detection with a 519 cm^{-1} frequency difference.

by selective LIF detection and by the knowledge acquired in our earlier work on the CaOH $\tilde{A}(020)-\tilde{X}(000)$ band, a large number of resolved LIF spectra were required in this work to establish definitive assignment of the vibronic species as well as the rotational quantum numbers, especially for the two nearly degenerate vibronic components, as mentioned before. The computer-controlled spectrometer in this laboratory provided good resolution ($\leqslant$0.13 Å) and high accuracy ($\leqslant$0.035 cm^{-1}). This was crucial for revealing the true fluorescence structures and intensity patterns which were otherwise severely blended or distorted. As an example, Figure 3 shows a resolved LIF spectrum obtained upon excitation of the CaOD $\tilde{A}(100)\ ^2\Pi_{1/2}-\tilde{X}(000)\ ^2\Sigma^+\ P_1(19\frac{1}{2})$ transition. If intensities were determined by Franck–Condon factors alone, the LIF features corresponding to the $\tilde{A}(100)-\tilde{X}(020)$

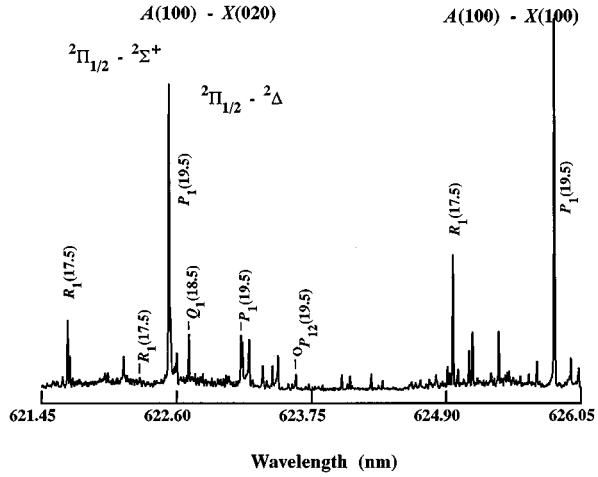

FIG. 3. Resolved LIF spectrum from excitation of the CaOD $\tilde{A}(100)\ ^2\Pi_{1/2}-\tilde{X}(000)\ ^2\Sigma^+\ P_1(19\frac{1}{2})$ transition.

transitions would be weaker than those corresponding to the $\tilde{A}(100)-\tilde{X}(100)$ transitions by at least 2 orders of magnitude. However, the difference in their relative intensities is actually less than 50%. This is an obvious indication of the (100)~(020) mixing in the upper states, which increases with increasing J values. It is also obvious in Fig. 3 that the $\tilde{A}(100)-\tilde{X}(020)\ ^2\Sigma^+$ transitions are much stronger than the $\tilde{A}(100)-\tilde{X}(020)\ ^2\Delta$ transitions. This is due, at least in part, to (100)~(020) mixing in the lower state, although this is much weaker than in the upper state; only the $\tilde{X}(020)\ ^2\Sigma^+$ component, and not the $\tilde{X}(020)\ ^2\Delta$ component, is connected to the $\tilde{X}(100)$ level by a Fermi resonance matrix element.

V. EFFECTIVE HAMILTONIAN MATRIX

As found in our preliminary treatment of the data sets for both isotopic molecules, it is impossible to fit the bands associated with the $\tilde{A}(100)$ and the $\tilde{A}(020)$ levels separately since they are linked by such a strong Fermi resonance interaction. Instead, it is necessary to conduct a global deperturbation employing a matrix that includes all six vibronic components and that simultaneously takes account of the Renner–Teller, spin–orbit and Fermi resonance interactions. Woodward *et al.*[8] performed a detailed matrix deperturbation of the interacting (100) and (020) $^2\Pi$ vibronic states of the NCO molecule. Our earlier work[5] on the CaOH $\tilde{A}\ ^2\Pi(100)(020)$ Fermi diad used essentially the same matrix as in Ref. 8 but included a much larger and more precise data set. In the present work, however, we have modified the matrix in order that the results are consistent (in terms of using exactly the same Hamiltonian operators) with our earlier results for the CaOH/CaOD $\tilde{A}\ ^2\Pi$ (000) and (010) vibrational levels.[6,15] In Refs. 8 and 5, the matrix was constructed in a case (a) basis set, but a rotational operator $\mathbf{N}$ ($=$**J-S**) was used for evaluation of the relevant matrix elements. In the present work, the rotational operator $\mathbf{R}$ ($=$**J-L-S-G**), instead of $\mathbf{N}$, has been used. In fact, all the matrix elements, except those for the Fermi resonance and g_{22} terms, have been rederived using the effective Hamiltonian described in our earlier publication[6] for the $\tilde{A}\ ^2\Pi(010)$ vibronic manifold. The case (a) basis set $|\Lambda l\Sigma, PJ\pm\rangle$ has been chosen with the symmetrized form

$$|(100)\ ^2\Pi_{3/2}, J\pm\rangle = 2^{-1/2}\{|1\ 0\ \tfrac{1}{2}, \tfrac{3}{2}\ J\rangle \pm |-1\ 0\ -\tfrac{1}{2}, -\tfrac{3}{2}\ J\rangle\}, \tag{3}$$

$$|(100)\ ^2\Pi_{1/2}, J\pm\rangle = 2^{-1/2}\{|1\ 0\ -\tfrac{1}{2}, \tfrac{1}{2}\ J\rangle \pm |-1\ 0\ \tfrac{1}{2}, -\tfrac{1}{2}\ J\rangle\}, \tag{4}$$

$$|(020)\kappa\ ^2\Pi_{3/2}, J\pm\rangle = 2^{-1/2}\{|1\ 0\ \tfrac{1}{2}, \tfrac{3}{2}\ J\rangle \pm |-1\ 0\ -\tfrac{1}{2}, -\tfrac{3}{2}\ J\rangle\}, \tag{5}$$

$$|(020)\mu\ ^2\Pi_{1/2}, J\pm\rangle = 2^{-1/2}\{|1\ 0\ -\tfrac{1}{2}, \tfrac{1}{2}\ J\rangle \pm |-1\ 0\ \tfrac{1}{2}, -\tfrac{1}{2}\ J\rangle\}, \tag{6}$$

$$|(020)\mu\ ^2\Pi_{3/2}, J\pm\rangle = 2^{-1/2}\{|-1\ 2\ \tfrac{1}{2},\ \tfrac{3}{2}\ J\rangle \pm |1\ -2\ -\tfrac{1}{2}, -\tfrac{3}{2}\ J\rangle\}, \tag{7}$$

$$|(020)\kappa\ ^2\Pi_{1/2}, J\pm\rangle = 2^{-1/2}\{|-1\ 2\ -\tfrac{1}{2}, \tfrac{1}{2}\ J\rangle \pm |1\ -2\ \tfrac{1}{2}, -\tfrac{1}{2}\ J\rangle\}, \tag{8}$$

where the upper and lower signs refer to e and f levels, respectively. The matrix thus consists of two independent 6×6 blocks. It is given in Table I. The subscripts 1 and 2 refer to the (100) and (020) vibrational levels, respectively. T_1 and T_2 are electronic-vibrational term values, and A_1, A_2, B_1, $B_2\cdots$ are conventional molecular constants.

An l-type doubling matrix element, $\mp 2^{1/2}(J+\frac{1}{2})q^v$, between the $(020)\kappa\ ^2\Pi_{1/2}$ and $\mu\ ^2\Pi_{1/2}$ vibronic components has been derived according to Eq. (13) in Ref. 6 and added into the matrix of the present work. This element was missing in the matrix of Refs. 5 and 8, as mentioned in Sec. I.

As in our earlier work,[5] the $g_{22}l^2$ terms have been chosen to replace the g_4 terms used in Ref. 8 to take into account the anharmonic effect on the vibrational energies. This approach is based on a description of the anharmonic corrections by Hougen and Jesson,[16] which is considered to be suitable for the present situation. The advantage of using the g_{22} terms for the $\tilde{A}(020)$ state is that the fitted value of g_{22} can be compared with the corresponding value for the $\tilde{X}$ (020) state, and can be used directly for estimation of the harmonic bending frequency.

There is a small change in the operator $B\mathbf{R}^2$ from Ref. 6, which is given here as

$$B\mathbf{R}^2 = (\mathbf{J}^2 - J_z^2 + \mathbf{S}^2 - S_z^2 - G_z^2) - (J_+S_- + J_-S_+). \tag{9}$$

The operator G_z^2 is now given explicitly in $B\mathbf{R}^2$ because it has different eigenvalues, 0 and 4, for different (020) basis states expressed in Eqs. (5)–(8). The main effect of including this operator will be on the value of g_{22} which will be now more suitable for comparison with the g_{22} value in the $\tilde{X}$ state. The centrifugal distortion terms (D, A_D, γ_D, and $\epsilon_D\omega_2$) for the (020) vibronic manifold have been correspondingly changed, however, these changes are very minor. The G_z^2 operator was not considered in Refs. 5 and 8.

The matrix elements for the Fermi resonance remain the same as those used in Refs. 5 and 8. They have somewhat different forms from those given by Hougen[10] because an uncoupled basis of zero order wave functions expressed in Eqs. (3)–(8) are used here. The terms containing the Renner parameter ϵ were derived from the Hamiltonian $H_{\text{Fermi}}\times H_{\text{Renner}}$, where H_{Fermi} connects vibrational states with $\Delta v_1=\pm1$, $\Delta v_2=\Delta v_3=0$, and H_{Renner} connects vibrational states with $\Delta v_1=\Delta v_3=0$, $\Delta v_2=\pm2$.

In addition to the results for CaOD, we also report in this paper the new results for the corresponding levels of CaOH obtained using the present Hamiltonian matrix and a substantially expanded data set that includes some high-J ($\leqslant 58\frac{1}{2}$) rotational lines and two new subbands, $\tilde{A}(020)\kappa\ ^2\Pi_{1/2,3/2}-\tilde{X}(020)\ ^2\Delta, ^2\Sigma^+$.

The rotational energies in excited bending vibrational levels of electronic $^2\Sigma$ and $^3\Sigma$ states have been studied in detail by Merer and Allegretti.[17] The matrix for $v_2=2$ in a $^2\Sigma$ electronic state in the case (b) representation, given in Table 3 of Ref. 17, was used for the CaOH/CaOD $\tilde{X}(020)$

TABLE I. Effective Hamiltonian matrix for the (100) and (020) $^2\Pi$ vibronic states of CaOH/CaOD with $x=J+\frac{1}{2}$ and $z=x^2$. The basis functions are defined by the symmetrized case (a) functions $|JP,\pm\rangle=2^{-1/2}\{|\Lambda l\Sigma,JP\rangle\pm|-\Lambda-l-\Sigma,J-P\rangle\}$. The upper and lower signs refer to the *e* and *f* levels, respectively. The subscripts 1 and 2 denote the (100) and (020) vibrational levels, respectively.

(100)		(020)			
$\lvert 1\,0\,\frac{1}{2}\rangle$	$\lvert 1\,0\,-\frac{1}{2}\rangle$	$\lvert 1\,0\,\frac{1}{2}\rangle$	$\lvert 1\,0\,-\frac{1}{2}\rangle$	$\lvert -1\,2\,\frac{1}{2}\rangle$	$\lvert -1\,2\,-\frac{1}{2}\rangle$
$T_1-\frac{1}{4}\epsilon^2\omega_2+g_K-\frac{1}{2}\gamma_1$ $+\frac{1}{2}A_1(1-\frac{1}{4}\epsilon^2)$ $+(B_1+\frac{1}{2}A_{D1})(z-2)$ $-D_1(z^2-3z+3)-\gamma_{D1}(z-\frac{3}{2})$	$-(z-1)^{1/2}[B_1-\frac{1}{2}\gamma_1$ $-2D_1(z-1)-\frac{1}{2}\gamma_{D1}z$ $\mp\frac{1}{2}q_1x]$	$2W_1-2\epsilon W_2$	0	$2\sqrt{2}W_2-\sqrt{2}\epsilon W_1$	0
	$T_1-\frac{1}{4}\epsilon^2\omega_2+g_K-\frac{1}{2}\gamma_1$ $-\frac{1}{2}A_1(1-\frac{1}{4}\epsilon^2)$ $+(B_1-\frac{1}{2}A_{D1})z-D_1(z^2+z-1)$ $\mp\frac{1}{2}(p_1+2q_1)x-\gamma_{D1}(z-\frac{1}{2})$	0	$2W_1-2\epsilon W_2$	0	$2\sqrt{2}W_2-\sqrt{2}\epsilon W_1$
		$T_2-\frac{3}{4}\epsilon^2\omega_2+g_K-\frac{1}{2}\gamma_2$ $+\frac{1}{2}A_2(1-\frac{3}{4}\epsilon^2)$ $+(B_2^0+\frac{1}{2}A_{D2})(z-2)$ $-D_2(z^2-3z+3)-\gamma_{D2}(z-\frac{3}{2})$	$-(z-1)^{1/2}[B_2^0-\frac{1}{2}\gamma_2$ $-2D_2(z-1)-\frac{1}{2}\gamma_{D2}z$ $\mp\frac{1}{2}q_2x]$	$\sqrt{2}\epsilon\omega_2+\sqrt{2}(z-4)\epsilon_D\omega_2$	$\pm\frac{1}{2}q^vx(2z-2)^{1/2}$ $-\epsilon_D\omega_2(2z-2)^{1/2}$
			$T_2-\frac{3}{4}\epsilon^2\omega_2+g_K-\frac{1}{2}\gamma_2$ $-\frac{1}{2}A_2(1-\frac{3}{4}\epsilon^2)$ $+(B_2^0-\frac{1}{2}A_{D2})z-D_2(z^2+z-1)$ $\mp\frac{1}{2}(p_2+2q_2)x-\gamma_{D2}(z-\frac{1}{2})$	$\pm\frac{1}{2}q^vx(2z-2)^{1/2}$ $-\epsilon_D\omega_2(2z-2)^{1/2}$	$\sqrt{2}\epsilon\omega_2+\sqrt{2}(z-2)\epsilon_D\omega_2$ $\mp\sqrt{2}xq^v$
				$T_2-g_K+4g_{22}-\frac{1}{2}\gamma_2$ $-\frac{1}{2}A_2(1-\frac{1}{2}\epsilon^2)$ $+(B_2^2-\frac{1}{2}A_{D2})(z-6)$ $-D_2(z^2-11z+35)-\gamma_{D2}(z-\frac{7}{2})$	$-(z-1)^{1/2}[B_2^2-\frac{1}{2}\gamma_2$ $-2D_2(z-5)-\frac{1}{2}\gamma_{D2}(z-4)]$
					$T_2-g_K+4g_{22}-\frac{1}{2}\gamma_2$ $+\frac{1}{2}A_2(1-\frac{1}{2}\epsilon^2)$ $+(B_2^2+\frac{1}{2}A_{D2})(z-4)$ $-D_2(z^2-7z+15)-\gamma_{D2}(z-\frac{5}{2})$

TABLE II. Matrix representation for $v_2=2$ in a $^2\Sigma^+$ electronic state. $x=J+\frac{1}{2}$; the upper/lower signs refer to e/f levels.

$\lvert^2\Delta(F_2)\rangle$	$\lvert^2\Delta(F_1)\rangle$	$\lvert^2\Sigma^+\rangle$
T_v+4g_{22} $+\left[B_\Delta-1/2\gamma\frac{1}{x}\right]\left[x\left(J+\frac{3}{2}\right)-4\right]$ $-D_\Delta\left[x\left(J+\frac{3}{2}\right)-4\right]^2$	$\gamma[(J-\frac{3}{2})(J+\frac{5}{2})]^{1/2}\frac{1}{x}$	$-q^v\left[x\left(J-\frac{1}{2}\right)\left(J+\frac{3}{2}\right)\left(J+\frac{5}{2}\right)\right]^{1/2}$ [a]
	T_v+4g_{22} $+\left[B_\Delta+1/2\gamma\frac{1}{x}\right]\left[x\left(J-\frac{1}{2}\right)-4\right]$ $-D_\Delta\left[x\left(J-\frac{1}{2}\right)-4\right]^2$	$q^v\left[x\left(J-\frac{3}{2}\right)\left(J-\frac{1}{2}\right)\left(J+\frac{3}{2}\right)\right]^{1/2}$ [b]
		$T_v+B_\Sigma x(J+1/2\mp1)\pm1/2\gamma(J+1/2\mp1)$ $-D_\Sigma x^2(J+1/2\mp1)^2$

[a]Only for f levels.
[b]Only for e levels.

state. A typographic error in the matrix for the $(02^00)\ ^2\Sigma$ level of Ref. 17 has been corrected. For clarification, the matrix used in this work is given in Table II. The expressions for the $\tilde{X}(000)\ ^2\Sigma^+$ level are the same as the diagonal matrix element for the $^2\Sigma^+$ state in Table II.

The dependence of the rotational constant B_v on bending vibrational quantum numbers v_2 and l can be expressed, according to Lide and Matsumura,[18] by

$$B_v=\bar{B}_e-\alpha_2(v_2+1)+\gamma_{22}(v_2+1)^2+\gamma_{ll}l^2, \tag{10}$$

where $\bar{B}_e=B_e-\alpha_1(v_1+\frac{1}{2})-\alpha_3(v_3+\frac{1}{2})$. It was indeed found in the least squares fits for both isotopomers that different B_v's must be used for the two components with $l=0$ and 2 of the $\tilde{X}(020)$ level, and they are labeled then as B_Σ and B_Δ, respectively, in the matrix of Table II. In a similar way, the basis states with $l=0$ and 2 for the $\tilde{A}\ ^2\Pi(020)$ level also have different B_v's, and these are labeled as B_2^0 and B_2^2 in the matrix of Table I. For the $^2\Pi$ electronic state, a further vibration–rotation correction to B values has been described by Brown;[19] this correction occurs for vibronic components of different ΛK and the same v_2 values, and its origin arises principally in third order perturbation theory, involving Renner–Teller, Fermi resonance and rotational operators. Brown has given the form for the correction as

$$\Delta B=\beta_{B,12}(v_1+\tfrac{1}{2})(v_2+1)(\Lambda K+1)+\beta_{B,32}(v_3+\tfrac{1}{2})(v_2+1)(\Lambda K+1), \tag{11}$$

where $\beta_{B,12}$ and $\beta_{B,32}$ are perturbation parameters. Referring to the basis functions defined in Eqs. (3)–(8), $\Lambda K=1$ for $l=0$ and $\Lambda K=-1$ for $l=\pm2$. The values of B_2^0 and B_2^2 will thus depend on the combined effects expressed in Eqs. (10) and (11).

VI. LEAST SQUARES FIT AND RESULTS

A weighted, nonlinear least squares fitting procedure employing the Hamiltonian matrices of Tables I and II was used to fit the complete data set for all the observed subbands for each isotopomer. The molecular constants and perturbation parameters for the $\tilde{A}(100)/(020)$ and $\tilde{X}(020)$ levels were allowed to vary simultaneously. The constants for the $\tilde{X}(000)$ level had been determined accurately by Ziurys *et al.*[20] for CaOH and by our earlier work[15] for CaOD, and were held fixed in the fits. The numbers of fitted rotational lines in respective subbands are given in Figs. 1(a) and 1(b). The total numbers of rotational lines included in the fits are 676 for CaOH and 635 for CaOD. The variances of the fits are $\hat{\sigma}^2=(1.199)^2$ and $\hat{\sigma}^2=(1.228)^2$ for CaOH and CaOD, respectively. The measurement uncertainty for most rotational lines was estimated to be 0.0035 cm^{-1}, which was used for assigning the weight ($w=0.0035^{-2}$) to rotational lines in the fit. It appears that the model used here has reproduced the observed quantities quite satisfactorily; however, the estimated variances are larger than unity because of small systematic discrepancies for a few of the branches. The measured line positions along with their quantum numbers J and residuals ($\bar{\nu}_{obs.}-\bar{\nu}_{calc.}$) obtained from the fits are listed in[21] PAPS Appendix A as Tables A1–A12. It is to be noticed that the two upper (020) vibronic components form an inverted $^2\Pi$ state and, therefore, the F_1/F_2 assignment is the opposite to that for the lower components. The molecular constants and perturbation parameters determined in the fits for both CaOH and CaOD are summarized in Table III.

Investigation of the $\tilde{A}(020)\kappa\ ^2\Pi_{1/2}$ vibronic component relied mainly on hot band excitation from the $\tilde{X}(020)\ ^2\Delta$ level; the $\kappa\ ^2\Pi_{1/2}-(020)\ ^2\Sigma^+$ subband was extremely weak for both isotopomers. The branch structure of this subband is referred to the schematic diagram in Fig. 2 of Ref. 14. The $\kappa\ ^2\Pi_{1/2}$ component was assigned as the F_2 component and its rotational structure conforms closely to Hund's case (b). This subband was difficult to measure and analyze owing to its weakness (low population in the lower state) and the unresolved spin–rotation splittings in the lower state combined with the K-type splittings in the upper state. Since the lower state has $^2\Delta$ symmetry, each rotational line is split into two lines by the l-type resonance in the lower state, which is

TABLE III. Molecular constants[a] of the (100) and (020) levels in the $\tilde{A}\ ^2\Pi$ and $\tilde{X}\ ^2\Sigma^+$ states of CaOH and CaOD.

	CaOH		CaOD	
	$\tilde{A}(100)$	$\tilde{A}(020)$	$\tilde{A}(100)$	$\tilde{A}(020)$
T_{ev}	16 626.922(1)	16 700.173(2)	16 614.005(2)	16 528.911(3)
A_v	67.165(3)	[67.095 1]	67.044(4)	[66.947 4]
$\lvert W_1\rvert$	10.3256(5)		5.2707(22)	
$\epsilon\omega_2$		−36.564 1(7)		−27.159 8(14)
g_K		[0.593 7]		[0.446 2]
g_{22}		7.531 4(10)		4.370 3(6)
B_v	0.338 906 1(41)	0.339 581 9(48) B_2^0	0.307 059 0(27)	0.309 396 0(78) B_2^0
		0.339 269 2(68) B_2^2		0.308 897 9(113) B_2^2
D_v	$0.377\ 0(17)\times10^{-6}$	$0.419\ 7(17)\times10^{-6}$	$0.253\ 6(34)\times10^{-6}$	$0.316\ 4(23)\times10^{-6}$
p^e	−0.044 05(7)	−0.045 45(9)	−0.039 29(10)	−0.041 54(9)
q^e	$-0.417\ 3(58)\times10^{-3}$	$-0.541\ 3(39)\times10^{-3}$	$-0.322\ 3(26)\times10^{-3}$	$-0.608\ 1(74)\times10^{-3}$
q^v		$-0.735\ 5(9)\times10^{-3}$		$-0.758\ 7(24)\times10^{-3}$
γ_v	[0.030 4]	[0.026 17]	[0.027 6]	[0.024 75]
A_{Dv}	$0.370(7)\times10^{-3}$	$-1.36(2)\times10^{-3}$	$0.195(8)\times10^{-3}$	$0.509(55)\times10^{-3}$
γ_D	$-0.537(40)\times10^{-5}$	$1.103(15)\times10^{-5}$	$1.178(91)\times10^{-5}$	$-0.219(38)\times10^{-5}$
$\epsilon_D\omega_2$		$-0.170(4)\times10^{-3}$		$0.276(17)\times10^{-3}$
	$\tilde{X}(100)$[b]	$\tilde{X}(020)$	$\tilde{X}(100)$[b]	$\tilde{X}(020)$
T_{ev}	609.015(10)	688.670(1)	604.903(7)	519.192(1)
g_{22}		6.086 7(12)		4.302 7(9)
B_v	0.332 19(3)	0.333 047(4) ($^2\Sigma$)	0.301 02(2)	0.303 396(4) ($^2\Sigma$)
		0.332 566(11) ($^2\Delta$)		0.303 113(15) ($^2\Delta$)
D_v	$[0.386\ 9\times10^{-6}]$	$0.415(2)\times10^{-6}(^2\Sigma)$	$0.283(10)\times10^{-6}$	$0.332(3)\times10^{-6}(^2\Sigma)$
		$0.468(6)\times10^{-6}(^2\Delta)$		$0.263(12)\times10^{-6}(^2\Delta)$
γ_v	[0.001 11]	[0.001 184]	[0.001 11]	[0.001 124]
q^v		$[-0.718\ 1\times10^{-3}]$		$[-0.762\ 1\times10^{-3}]$

[a]All values are in cm^{-1}; values in parentheses are 1σ standard deviations in units of the last significant digit of the corresponding constant. $W_2=0$ was fixed.
[b]From Ref. 14.

negligible, and by the K-type doubling in the upper state, which is large. The splitting is resolved at low-J', but decreases as J' increases and becomes zero at $J'=16\frac{1}{2}$ for CaOD, and then opens again as J' further increases. This may be seen later in Fig. 4(b) which shows the change in sign of the K splittings $(\bar{\nu}_e-\bar{\nu}_f)$ in $\kappa\ ^2\Pi_{1/2}$ at $J'=16\frac{1}{2}$. A similar situation occurs for CaOH. Although this is a case (b)–case (b) transition, relative intensities between the main and satellite branches change in a complicated fashion due to quantum interference. For these reasons, the data for this subband were assigned lower weights ($w=0.01^{-2}$). For CaOD, there was an additional difficulty in the fit caused by the near degeneracy of $\tilde{A}(100)\ ^2\Pi_{1/2}$ and $\tilde{A}(020)\kappa\ ^2\Pi_{3/2}$. The strong J-dependent interaction between the two components has not been satisfactorily modeled by the present effective Hamiltonian. As a consequence, the data for the nominal $\tilde{A}(020)\kappa\ ^2\Pi_{3/2}-\tilde{X}(000)\ ^2\Sigma^+$ subband included in the fit have been restricted to $J'\leqslant34\frac{1}{2}$ to avoid large residuals and contamination of molecular constants.

The parameters γ and q^v in the $\tilde{X}(020)$ state could not be reliably determined and were, hence, constrained at the values for the $\tilde{X}(010)$ level. This is because the spin–rotation splittings in the $\tilde{X}(020)\ ^2\Delta$ and $^2\Sigma^+$ levels are very small and the l-type doubling in the $\tilde{X}(020)\ ^2\Delta$ state is negligible; unfortunately, the corresponding subbands are too weak to permit a sub-Doppler investigation. Nevertheless, the principal parameters for the $\tilde{X}(020)$ state, $T_{\rm ev}$, B_v, D_v, and g_{22}, have been well determined for both isotopomers. The assumed values of γ and q^v should be quite reasonable, with any errors having negligible effect on the fits.

VII. DISCUSSION AND FURTHER RESULTS

A. Values of g_{22} and Fermi resonance in the $\tilde{X}$ state

As seen from the matrix in Table I, the parameter g_K is highly correlated with g_{22}. Since g_K had been determined accurately for both CaOH and CaOD from investigations of the $\tilde{A}(010)$ state,[6] its value was held fixed while g_{22} was allowed to vary. The fitted values of g_{22} for both CaOH and CaOD in the $\tilde{A}$ state are consistent with those in the $\tilde{X}$ state, as shown in Table III. However, small differences have been noticed. The g_{22} value for the CaOH $\tilde{A}$ state is larger by ~20% than that in the $\tilde{X}$ state, while for CaOD, g_{22} has nearly the same value for the $\tilde{A}$ and $\tilde{X}$ states. This situation merits further discussion. In the $\tilde{X}$ state, the Fermi interaction between the (100) and (020) levels was not taken into account in the matrix deperturbation of the observed bands. For CaOH, the (100) level is lower than the (02^00) level by ~80 cm^{-1} while the (02^20) level is higher than (02^00) by 24.3 cm^{-1}. The Fermi resonance operator only connects the (100) and (02^00) levels (selection rule $\Delta l=0$). The effect of this interaction on vibrational energies is certainly not negligible.

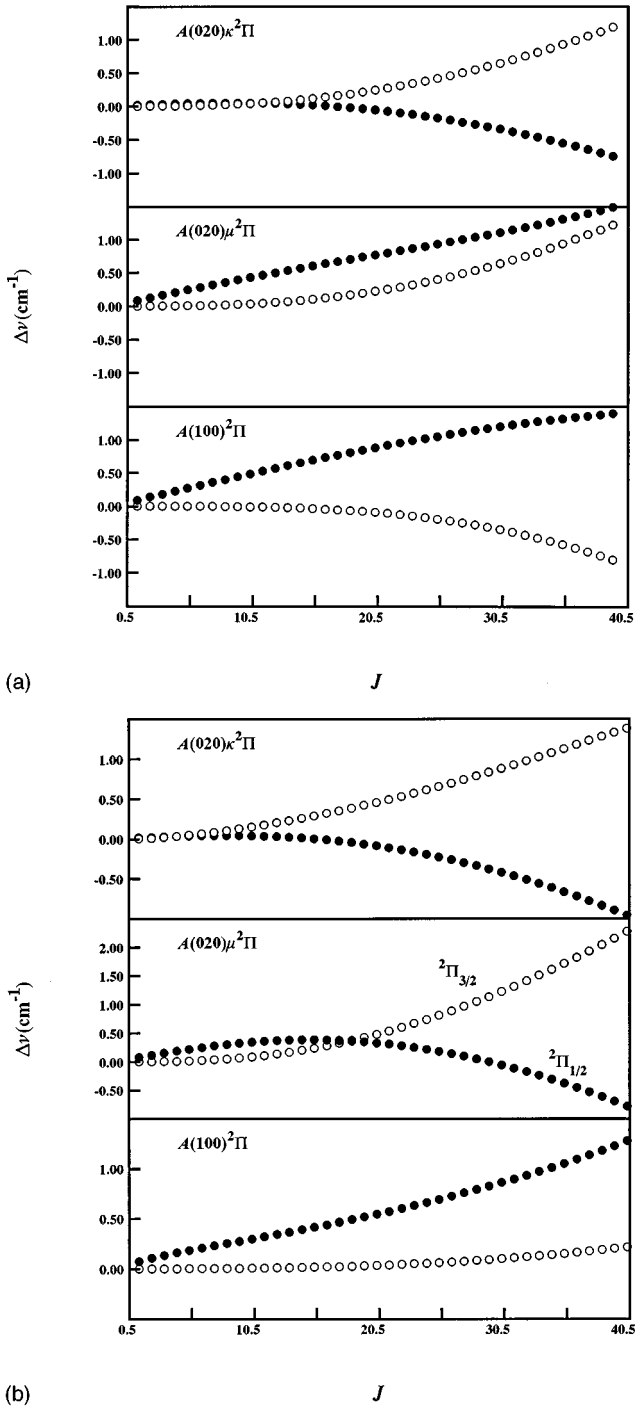

FIG. 4. K-type doublings, $\Delta\bar{\nu}=\bar{\nu}_e-\bar{\nu}_f$, in the $\tilde{A}\ ^2\Pi$ (020) and (100) vibronic states: (a) for CaOH, (b) for CaOD. ● For $^2\Pi_{1/2}$ levels; ○ for $^2\Pi_{3/2}$ levels.

However, since the unperturbed energies of the $\tilde{X}(100)$ and (020) levels could not be predicted accurately owing to lack of zero-order vibrational information, it was impossible to treat this interaction rigorously in a matrix approach. Nevertheless, since the two electronic states have quite similar potentials, a reasonable approximation is to assume that the Fermi resonance parameter W for $\tilde{X}\ ^2\Sigma^+$ has the same value as W_1 for the $\tilde{A}$ state. The interaction can then be treated by solving a simple secular equation

TABLE IV. (a) Molecular parameters[a] for CaOH/CaOD in the $\tilde{A}\ ^2\Pi$ state. (b) Molecular parameters[a] for CaOH/CaOD in the $\tilde{X}\ ^2\Sigma^+$ state.

(a)	CaOH	CaOD
ν_1	628.487 1(15)	618.774 7(23)
ω_2^0	358.65 2(3)	272.58 2(3)
x_{22}^0	−3.892(3)	−2.871(3)
$\epsilon\omega_2$	−35.662 2(19)	−26.560 5(31)
ϵ	−0.097 3	−0.095 4
$\hat{g}_4$	−0.100 2(3)	−0.066 6(5)
$\lvert k_{122}\rvert$	2.027×10^{75}	0.780×10^{75}
$\lvert\phi_{122}\rvert$	29.205 2(14)	14.907 8(62)
α_2	0.001 164(9)	−0.000 001(13)
γ_{22}	0.000 086(5)	0.000 045(6)
γ_{ll}	−0.000 078(4)	−0.000 125(5)
(b)	CaOH	CaOD
ν_1	614.79	603.59
G_{020}^0	682.90	520.51
ω_2^0	349.34	265.49
x_{22}^0	−3.95	−2.61
g_{22}	7.53	3.97
α_2	0.001 093(6)	−0.000 011(12)
γ_{22}	0.000 112(3)	0.000 048(5)
γ_{ll}	−0.000 120(3)	−0.000 071(4)

[a]All parameters are in unit of cm^{-1} except that ϵ is dimensionless and k_{122} is in unit of $(kg^{-3/2}\ m^{-4})$. $\epsilon\omega_2$ and ϵ are the harmonic Renner–Teller parameters.

$$\begin{vmatrix} G^0(100)-G & 2W \\ 2W & G^0(02^00)-G \end{vmatrix}=0. \tag{12}$$

Here, $G^0(100)$ and $G^0(02^00)$ are the unperturbed energies and G is the perturbed energy, which has two known values; $2W$ is the perturbation matrix element originating from the Fermi resonance. Employing the deperturbed energies obtained from the above calculation, the deperturbed g_{22} value is determined as $g_{22}=7.53\ cm^{-1}$; this is an *increase* from the perturbed value of 6.09 cm^{-1} to a value that is essentially identical to the $\tilde{A}$ state g_{22} value. In the CaOD $\tilde{X}$ state, the (100) level is higher than the (02^00) level by ~86 cm^{-1}. Using the same approach, the deperturbed g_{22} value is determined as $g_{22}=3.97\ cm^{-1}$; there is now a *decrease* from the perturbed value of 4.30 cm^{-1} to a value that is smaller by ~10% than the $\tilde{A}$ state g_{22} value. From these results, it is apparent that a somewhat smaller correction would lead to deperturbed g_{22} values that are slightly less than those of $\tilde{A}\ ^2\Pi$ for *both* isotopomers. Hence, it may be deduced that the values of the Fermi resonance parameter in the $\tilde{X}$ state should be slightly smaller than those in the $\tilde{A}$ state for both CaOH and CaOD. Nevertheless, the deperturbed g_{22} values obtained above for $\tilde{X}\ ^2\Sigma^+$ using $W\approx W_1(\tilde{A}\ ^2\Pi)$ are considered more reliable than the perturbed values, and these are given in Table IV(b).

B. Vibrational parameters for the $\tilde{A}$ and $\tilde{X}$ states and vibrational dependence of $\epsilon\omega_2$

More important results obtained from the above treatment of the Fermi interactions in the $\tilde{X}$ state are, of course, the unperturbed vibrational term values: $G^0(100)=614.79$,

$G^0(02^00)=682.90$ cm^{-1} for CaOH, and $G^0(100)=603.59$, $G^0(02^00)=520.51$ cm^{-1} for CaOD. These deperturbed vibrational term values and g_{22} values of the $\tilde{X}$ state are believed to be more reliable than the perturbed values listed in Table III, and will be used for further calculations in this work. Of course, the above corrections do not imply any change in the quality of the matrix deperturbation of the observed bands described earlier in Secs. V and VI because the $\tilde{X}(100)\sim(020)$ Fermi resonance is J and parity independent and, hence, will not affect the values of B_v, D_v, and γ_v.

As for the treatment of the $\tilde{A}(010)$ state,[6] the Renner–Teller parameter ϵ was held fixed, ϵ(CaOH)$=-0.100$ and ϵ(CaOD)$=-0.098$, and $\epsilon\omega_2$ was allowed to vary, here for the $\tilde{A}(020)$ state. The spin–orbit constant A_2 is closely correlated with $\epsilon\omega_2$, and was constrained at the value for the $\tilde{A}(010)$ state.[6] The values of $\epsilon\omega_2$ were determined for both isotopomers by the least squares fits. There is a small increase in magnitude for $\epsilon\omega_2$ as v_2 increases from $v_2=1$ to $v_2=2$; the changes are $-0.3007(9)$ and $-0.1997(15)$ cm^{-1} for CaOH and CaOD, respectively. These small increases may be understood as a vibrational dependence of the Renner–Teller effect. Brown and Jorgensen[22,23] introduced a $\hat{g}_4$ term to account for such dependence. This term originates from the anharmonic quartic potential and has the form of $\hat{g}_4 q_2^4 \sigma_z$. q_2 is a dimensionless normal coordinate associated with the bending vibration, and σ_z is a Pauli matrix. According to Ref. 23, its matrix elements can be evaluated using

$$\langle q_2^4\sigma_z\rangle_{v_2,v_2}=\tfrac{3}{2}(v_2+1)[(v_2+1)^2-K^2]^{1/2}. \tag{13}$$

Considering this vibrational dependence, the Renner–Teller parameter $\epsilon\omega_2$ determined in the least squares fits may be written as $\epsilon\omega_2+6\hat{g}_4$ for $\tilde{A}(010)$ and $\epsilon\omega_2+9\hat{g}_4$ for $\tilde{A}(020)$. Thus the parameter $\hat{g}_4$ can be directly calculated from the difference between the fitted $\epsilon\omega_2$ values for $\tilde{A}(010)$ and $\tilde{A}(020)$, and its calculated values are $\hat{g}_4=-0.1002(3)$ and $-0.0666(5)$ cm^{-1} for CaOH and CaOD, respectively. These $\hat{g}_4$ values appear quite reasonable in that the anharmonicity of the bending vibration in CaOH is markedly larger than that in CaOD. Jarman and Bernath[24] obtained $\hat{g}_4=-0.038\,62(9)$ cm^{-1} for the CaOD $\tilde{C}\,^2\Delta$ electronic state, which is comparable with the present result. With $\hat{g}_4$ now known from the preceding discussion, it is possible to obtain the ''harmonic'' Renner–Teller parameter $\epsilon\omega_2$, excluding the anharmonic $\hat{g}_4$ contributions; estimates of $\epsilon\omega_2=-35.6622(19)$ cm^{-1} for CaOH and $\epsilon\omega_2=-26.5605(31)$ cm^{-1} for CaOD are obtained. Although the fitted $\epsilon\omega_2$ value is affected by the assumed value of the spin–orbit constant A_2, test fits have shown that when the A_2 value was changed by an amount extrapolated from the A values of the $\tilde{A}(000)$ and (010) levels, the change of the fitted $\epsilon\omega_2$ value for $\tilde{A}(020)$ was smaller than 0.015 cm^{-1} for CaOH. For CaOD, such change was even smaller. Hence, it can be concluded that the calculated values for $\hat{g}_4$ and the harmonic $\epsilon\omega_2$ are quite reliable.

The fundamental frequency of the Ca–O stretching vibration in the $\tilde{A}\,^2\Pi$ state can now be calculated from the (000) and (100) term values: $\nu_1=628.4871(15)$ cm^{-1} for CaOH and $\nu_1=618.7747(23)$ cm^{-1} for CaOD. Here, the $\tilde{A}(000)$ term value has been corrected by $-\frac{1}{4}\epsilon^2\omega_2+g_K$.

Using the term values of the $v_2=0$, 1 and 2 levels, and the expression for the vibrational term values referred to the (000) level[25]

$$G_0(v_1v_2v_3)=\sum_i \omega_i^0 v_i+\sum_i\sum_{k\geqslant i} x_{ik}^0 v_i v_k + \sum_i\sum_{k\geqslant i} g_{ik} l_i l_k+\cdots \tag{14}$$

ω_2^0 and x_{22}^0 for the $\tilde{A}$ and $\tilde{X}$ states of the two isotopomers were calculated; all quantities obtained in this section are summarized in Table IV. With the approximation

$$\omega_2\approx\omega_2^0-2x_{22}^0, \tag{15}$$

the harmonic frequency of the $\tilde{A}$ state bending vibration may be estimated as $\omega_2=366.435$ and 278.325 cm^{-1} for CaOH and CaOD, respectively. Using these ω_2 values and the harmonic $\epsilon\omega_2$ values, the harmonic Renner parameters ϵ may be calculated, yielding $\epsilon=-0.0973$ for CaOH and $\epsilon=-0.0954$ for CaOD.

Following the same approach, the harmonic bending frequency in the $\tilde{X}$ state was estimated as $\omega_2=357.23$ and 270.71 cm^{-1} for CaOH and CaOD, respectively. Here, the corrected $\tilde{X}$ state (020) term values and g_{22} values were used, as calculated above. The harmonic frequency of the Ca–O stretch vibration in the $\tilde{X}$ state is difficult to estimate although the excited levels up to $v_1=4$ for CaOH and $v_1=3$ for CaOD have been observed via dispersed LIF by our earlier work.[14] This is due to the existence of the Fermi resonance. The deperturbed term values of the (100) level have been estimated in the preceding section. However, when the quantum number v_1 increases further, more levels are involved into the Fermi polyads: (200)$\sim$(120)$\sim$(040), (300)$\sim$(220)$\sim$(140)$\sim$(060), etc. These interactions will significantly affect the level positions and can not be estimated easily. Therefore, the term values $G^0(100)$ calculated in the preceding section are considered the best approximation for the harmonic frequency ω_1 for CaOH and CaOD.

C. Fermi resonance parameters and cubic force constants in the $\tilde{A}$ state

The magnitude of the Fermi resonance parameter W_1 has been well determined for both CaOH and CaOD; however, the sign of W_1 could not be obtained. The second parameter, W_2, could not be determined by the fit for either isotopomer, and was fixed at a value of zero. This can be understood in terms of the moderate size of the Renner–Teller parameter in the CaOH/CaOD $\tilde{A}\,^2\Pi$ state; W_2 becomes significant only when the Renner–Teller effect is very strong. Even in the $\tilde{X}\,^2\Pi$ states of NCO[8] and BO_2,[26] where the vibronic couplings are relatively strong, $\epsilon\omega_2=-75.91$ and -85.7 cm^{-1}, respectively, W_2 was still not determined. The essentially zero value of W_2 indicates that $(k'_{122}-k''_{122})$ is close to zero, according to Eq. (2). Thus W_1 may be expressed by

$$W_1 = k_{122}(\hbar/4\pi c\omega_2)(\hbar/4\pi c\omega_1)^{1/2}. \quad (16)$$

Employing the $\tilde{A}$ state ω_2 value obtained in the previous section, and assuming $\omega_1 \approx \nu_1$, the magnitude of the anharmonic force constant k_{122} may be obtained: $|k_{122}| = 2.027\times10^{75}$ and 0.7799×10^{75} kg$^{-3/2}$ m^{-4} for CaOH and CaOD, respectively; these constants are the coefficients in the normal coordinate expansion of the potential energy function. More usually, the Fermi resonance parameter is employed as a direct measure of the anharmonic force constant ϕ_{122} in the dimensionless normal coordinate space,

$$W_1 = 8^{-1/2}\phi_{122}. \quad (17)$$

Equation (17) yields magnitudes of ϕ_{122} as 29.2052(14) and 14.9078(62) cm^{-1} for CaOH and CaOD, respectively. Here, we have defined the relevant cubic term in the potential function as $k_{122}Q_1Q_2^2$ in the normal coordinates and as $\phi_{122}q_1q_2^2$ in the dimensionless coordinates with $q_i = (2\pi c\omega_i/\hbar)^{1/2}Q_i$.

As is well known, the vibration–rotation interaction constant α_2 also contains information on the cubic anharmonic force constants ϕ_{n22}. The relation has been formulated by Nielsen[27] as

$$\alpha_2 = \frac{B_e^2}{\omega_2}\left\{1 + 4\sum_{n=1,3}\frac{\zeta_{2n}^2\omega_2^2}{\omega_n^2-\omega_2^2}\right\} - (2B_e)^{3/2}\left\{\frac{\zeta_{23}\phi_{122}}{\omega_1^{3/2}} + \frac{\zeta_{21}\phi_{322}}{\omega_3^{3/2}}\right\}, \quad (18)$$

where ζ_{2n} are the Coriolis coupling constants. A calculation of ϕ_{122} from the experimental α_2 values may be carried out as follows. The first term on the right-hand side of Eq. (18) is exactly equal to half of the absolute value of the l-type doubling constant q^v. The values of q^v in the CaOH/CaOD $\tilde{A}$ state have been determined from investigations of the (010) and (020) levels. The q^v values obtained from the (010) level[6] will be used here since the (010) vibronic manifold is simpler than the (100)/(020) manifold and was slightly better fitted. In the second term on the right-hand side of Eq. (18), $\zeta_{21}/\omega_3^{3/2}$ is smaller than $\zeta_{23}/\omega_1^{3/2}$ by a factor of 89 for CaOH and 44 for CaOD (the values of ω_n, ζ_{2n}, and B_e are given in Table VII). Hence, the ϕ_{322} term is expected to be much smaller than the ϕ_{122} term and may be neglected at present. Employing the α_2 values obtained in the next section, the following estimates are obtained: $\phi_{122} = -22.9$ cm^{-1} for CaOH and $\phi_{122} = 12.0$ cm^{-1} for CaOD. The magnitudes of ϕ_{122} evaluated from α_2 are in reasonably good agreement with those evaluated from W_1. The former are somewhat smaller than the latter. This is most likely caused by neglect of the ϕ_{322} term; the constant ϕ_{322} may be considerably larger than ϕ_{122} and have an opposite sign. The calculations using α_2 values have also given the signs for ϕ_{122}, which are not available from W_1. In Sec. VIII, the corresponding force constants f_{122} and f_{322} in the curvilinear internal coordinate expansion of the potential function are calculated from the α_2 values. Since f_{122} and f_{322} are isotopically invariant, both constants can be evaluated employing α_2 values of the two isotopic molecules. A nonlinear transformation would produce values for ϕ_{122} and ϕ_{322} from both harmonic constants ($f_{11}, f_{22}, f_{33}, f_{13}$) and anharmonic constants (f_{122} and f_{322}); the harmonic force field in the curvilinear coordinates gives contributions to the anharmonic force constants in the normal coordinates,[28] as will be described later in Sec. VIII. This would give a better verification of the results obtained from the Fermi resonance and, particularly, give an explanation for the large difference between the W_1 values in CaOH and in CaOD.

D. Vibrational dependence of rotational constants

The parameters that govern the dependence of the rotational constant B_v on the bending vibrational quantum numbers v_2 and l can now be calculated using the fitted B_v values for the $v_2 = 0$, 1, and 2 levels and Eq. (10). For the $\tilde{X}\,^2\Sigma^+$ electronic state the calculations are straightforward, resulting in $\alpha_2 = 0.001\,093(6)$, $\gamma_{22} = 0.000\,112(3)$, and $\gamma_{ll} = -0.000\,120(3)$ cm^{-1} for CaOH, and $\alpha_2 = -0.000\,011(12)$, $\gamma_{22} = 0.000\,048(5)$, and $\gamma_{ll} = -0.000\,071(4)$ cm^{-1} for CaOD. It is seen immediately that the parameter α_2 in CaOD is essentially zero while γ_{22} and γ_{ll} for CaOD are relatively large, being about half of those for CaOH. It is obvious that the parameter α_2 is much more sensitive to isotopic substitution than the other two parameters, γ_{22} and γ_{ll}. This behavior is strikingly similar to that occurring in the alkali metal hydroxides.[18] More detailed discussion on these parameters will be given in Sec. VIII. For the $\tilde{A}$ state, the situation becomes more complicated owing to the effect of the new vibration–rotation correction to the $B(020)$ values described by Eq. (11). However, an examination of Eq. (11) and the basis functions defined in Eqs. (5)–(8) revealed that the new vibration–rotation correction only affects the value of B_2^0 and has no effect on B_2^2 because of $\Lambda K + 1 = 0$ for $l = \pm 2$. Therefore, B_2^2 can still be expressed solely by Eq. (10). The magnitude of B_2^0 relative to B_2^2 in the $\tilde{A}$ state still follows the same trend seen in the $\tilde{X}$ state so that the new correction may only have a minor effect on B_2^0; this effect might have significant impact on γ_{ll} but should have minimal impact on α_2 and γ_{22}. Since only α_2 and γ_{22}, and not γ_{ll}, will be involved in the calculations of B_e, it was decided to ignore the new correction terms of Eq. (11) in the expression for B_2^0. For the $\tilde{A}(010)$ state,[6] the mean of the B values for $^2\Delta$ and $^2\Sigma$ vibronic components was used. The results for the $\tilde{A}$ state are as follows: $\alpha_2 = 0.001\,164(9)$, $\gamma_{22} = 0.000\,086(5)$, and $\gamma_{ll} = -0.000\,078(4)$ cm^{-1} for CaOH; $\alpha_2 = -0.000\,001(13)$, $\gamma_{22} = 0.000\,045(6)$, and $\gamma_{ll} = -0.000\,125(5)$ cm^{-1} for CaOD. The uncertainties of γ_{ll} may actually be larger than given in the parentheses. As in the $\tilde{X}$ state, α_2 is essentially zero for CaOD in the $\tilde{A}$ state. These results are summarized in Table IV. In a recent publication,[29] Fletcher *et al.* reported an investigation of pure rotational spectra in the vibrationally excited ground state of alkaline earth monohydroxides. The B_v values of the CaOH $\tilde{X}(02^00)$, (02^20), (010), and (100) levels obtained from the millimeter wave spectroscopy[29] are in excellent agreement with the results obtained in this work

and our earlier work.[6,14] The values of α_2, γ_{22}, and γ_{ll} in the CaOH $\tilde{X}$ state thus agree very well between the results of the two laboratories.

E. *K*-type doublings in the $\tilde{A}$ state

The *K*-type doublings in the $\tilde{A}(100)/(020)\ ^2\Pi$ manifold are complicated due to the existence of the Fermi resonance. In general, the present model reproduces the doublings very satisfactorily for both isotopomers. The fitted values of p^e and q^v are very close to those for the $\tilde{A}(000)$[15] and (010)[6] levels; however, q^e for the $\tilde{A}(020)$ level is noticeably larger in magnitude than might be expected for both CaOH and CaOD. There is no obvious explanation for this result. As pointed out in Ref. 6, the definition of the *l*-type doubling operator used in the present work removes the v_2 dependence from the constant q^v. Indeed, the q^v value obtained from the $\tilde{A}(020)$ level is in very good agreement with that from the $\tilde{A}(010)$ level for both CaOH and CaOD.

Figures 4(a) and 4(b) illustrate the *K*-type doublings, defined as $\Delta\bar{\nu}=\bar{\nu}_e-\bar{\nu}_f$, in the six vibronic components for CaOH and CaOD, respectively. Figure 4(a) was presented in our previous publication,[5] but for ease of comparison, it is reproduced here. For CaOD, the *K*-type doublings are not severely affected by the Fermi resonance although the $(100)\ ^2\Pi_{1/2}$ and the $(020)\kappa\ ^2\Pi_{3/2}$ components perturb each other strongly. This is because the two components have similar *K* doublings, as shown in Fig. 4(a) for CaOH in which the corresponding components encounter minimal Fermi perturbations. The effect of the Fermi interaction on the *K* doublings is manifested most dramatically in the $(100)\ ^2\Pi_{3/2}$ and $(020)\mu\ ^2\Pi_{1/2}$ components of CaOH. These two components have very different *K* splittings and interact with each other very strongly. The $(100)\ ^2\Pi_{3/2}$ component normally has negligible *K* doublings, but now has fairly large negative $\Delta\bar{\nu}$. The $(020)\mu\ ^2\Pi_{1/2}$ component has steadily increasing positive $\Delta\bar{\nu}$ with increasing *J* while the corresponding component of CaOD exhibits a sign change of $\Delta\bar{\nu}$ at $J=18\frac{1}{2}$.

It should be emphasized that the labeling of some vibronic states is rather difficult because of heavy mixing. The labels that represent leading characters at $J=1\frac{1}{2}$ have been chosen. Table V lists mixing percentages for each eigenstate of CaOD at $J=1\frac{1}{2}$, $20\frac{1}{2}$, and $40\frac{1}{2}$. As shown in the table, the mixing between $(100)\ ^2\Pi_{1/2}$ and $(020)\kappa\ ^2\Pi_{3/2}$ increases as *J* increases and the two vibronic states switch leading characters after $J=40\frac{1}{2}$. For CaOH, the $(020)\mu\ ^2\Pi_{3/2}$ and $(100)\ ^2\Pi_{3/2}$ states are completely mixed at all *J* values. As *J* increases, the interactions of $(020)\mu\ ^2\Pi_{1/2}$ with both $(020)\mu\ ^2\Pi_{3/2}$ and $(100)\ ^2\Pi_{3/2}$ become rapidly stronger and cause complete mixing at $J\geqslant 30\frac{1}{2}$. The mixing percentages for the corresponding eigenstates of CaOH were listed in Table IV of Ref. 5, and are not given here since only very small changes occurred in the mixing percentages after the new fit by the present work.

F. Isotope relation of molecular constants for CaOH and CaOD

It is of interest to examine the isotopic behavior of the parameters determined for the (100) and (020) levels. Results are collected in Table VI, which also includes isotopic ratios of the parameters for the (000) and (010) levels which were determined earlier in Refs. 6 and 15, respectively; the latter are useful in order to gauge the self-consistency of the results obtained in our work. In Table VI, only the ratios of the molecular constants that were determined by the least squares fits are given. The isotope ratio of q^e in the $\tilde{A}(020)$ state is not included in Table VI because the fitted q^e values in $\tilde{A}(020)$ are not considered to have been well deperturbed.

For diatomic molecules, it has been shown[30] that the ratios of some molecular constants at equilibrium (p_e/B_e, q_e/B_e^2, A_{De}/B_e, and γ_e/B_e) are isotopically invariant. The above results clearly demonstrate that the isotope relations of the parameters, B_v, p^e, q^e, and γ_v, are still well satisfied in the range of $v_1\leqslant 1$ and $v_2\leqslant 2$ for a linear triatomic molecule, although the situation becomes much more complicated owing to the existence of more vibrational modes. It is also obvious that the isotope ratios of the parameters are in excellent agreement between the $\tilde{X}$ and $\tilde{A}$ states. The overall consistency shown in the above ratios lends strong confidence to the data sets and the global matrix deperturbation approach used in the present work. The value of $B_v^{\mathrm{D}}/B_v^{\mathrm{H}}$ increases slowly as v_2 increases in both the $\tilde{X}$ and $\tilde{A}$ states, which is in accord with the different v_2 dependence of the rotational constants in the two isotopomers.

The correlation between A_D and γ in a diatomic $^2\Pi$ state is well known;[31,32] such correlation also exists in the $\tilde{A}(100)$ and (020) levels of a triatomic $^2\Pi$ state. Therefore, in the practical fits, γ_1 and γ_2 were held fixed at the values for the $\tilde{A}(000)$[15] and (010)[6] levels, respectively, and A_{D1} and A_{D2} were allowed to vary. As seen in Table III, the fitted values of some of the high-order parameters (A_D, γ_D, and $\epsilon_D\omega_2$) are not reasonable in magnitude or sign. This situation is very difficult to avoid since the interactions, especially at high *J*, are too strong to give a perfect treatment.

VIII. EQUILIBRIUM STRUCTURE AND FORCE FIELD

In our earlier publication,[6] an attempt was made to determine the molecular equilibrium structure and force field for the $\tilde{X}\ ^2\Sigma^+$ state of CaOH/CaOD. After analyzing the $\tilde{A}(100)/(020)-\tilde{X}(020)$ bands in the present work, more accurate constants for the $\tilde{X}(020)$ level were determined and the effect of the $\tilde{X}(100)-(020)$ Fermi interactions was better understood. In consequence, the parameters ω_1, ω_2, and B_e for the $\tilde{X}$ state have now been more reliably determined. For the $\tilde{A}$ state, these parameters have also been determined with the same quality as for the $\tilde{X}$ state. New calculations of equilibrium bond lengths and force constants are now performed for both the $\tilde{X}$ and $\tilde{A}$ states.

Despite much effort in this and some other laboratories, searches for the excited levels of the ν_3 (O–H stretch) mode have not been successful. In fact, the excited O–H stretch vibration has not been observed for any metal monohydrox-

TABLE V. Mixing percentages of the $^2\Pi$ vibronic states of CaOD.

			e levels			
$J=1\frac{1}{2}$	16 649.218	16 594.978	16 581.825	16 581.004	16 490.795	16 479.450
$^2\Pi_{3/2}$	98.14	0.00	0.02	1.71	0.13	0.00
$\kappa\ ^2\Pi_{1/2}$	0.00	80.23	6.51	0.44	0.01	12.81
$^2\Pi_{1/2}$	0.01	5.92	90.97	2.14	0.00	0.97
$\kappa\ ^2\Pi_{3/2}$	1.75	0.04	1.90	73.00	23.26	0.04
$\mu\ ^2\Pi_{3/2}$	0.10	0.02	0.60	22.70	76.48	0.08
$\mu\ ^2\Pi_{1/2}$	0.00	13.78	0.00	0.00	0.11	86.10
$J=20\frac{1}{2}$	16 783.981	16 731.233	16 716.794	16 713.969	16 627.660	16 612.828
$^2\Pi_{3/2}$	97.24	0.43	0.00	2.20	0.10	0.03
$\kappa\ ^2\Pi_{1/2}$	0.01	75.45	0.04	11.79	0.90	11.81
$^2\Pi_{1/2}$	0.84	3.39	67.57	27.21	0.16	0.83
$\kappa\ ^2\Pi_{3/2}$	1.79	4.84	24.61	45.96	18.52	4.28
$\mu\ ^2\Pi_{3/2}$	0.11	2.67	7.46	12.68	67.96	9.13
$\mu\ ^2\Pi_{1/2}$	0.02	13.22	0.31	0.17	12.36	73.92
$J=40\frac{1}{2}$	17 165.737	17 116.296	17 097.053	17 093.172	17 014.069	16 991.164
$^2\Pi_{3/2}$	94.96	0.97	0.12	3.82	0.06	0.07
$\kappa\ ^2\Pi_{1/2}$	0.03	67.65	4.38	15.65	1.33	10.95
$^2\Pi_{1/2}$	2.91	0.96	49.85	45.20	0.40	0.69
$\kappa\ ^2\Pi_{3/2}$	1.90	11.39	36.00	29.30	12.25	9.16
$\mu\ ^2\Pi_{3/2}$	0.12	6.61	8.73	6.00	59.97	18.57
$\mu\ ^2\Pi_{1/2}$	0.08	12.41	0.92	0.02	26.01	60.56
			f levels			
$J=1\frac{1}{2}$	16 649.218	16 594.965	16 581.752	16 581.002	16 490.794	16 479.373
$^2\Pi_{3/2}$	98.14	0.00	0.03	1.70	0.13	0.00
$\kappa\ ^2\Pi_{1/2}$	0.00	80.31	6.39	0.49	0.01	12.80
$^2\Pi_{1/2}$	0.01	5.85	90.57	2.60	0.00	0.97
$\kappa\ ^2\Pi_{3/2}$	1.75	0.05	2.28	72.62	23.26	0.04
$\mu\ ^2\Pi_{3/2}$	0.10	0.02	0.73	22.58	76.48	0.08
$\mu\ ^2\Pi_{1/2}$	0.00	13.77	0.00	0.00	0.11	86.12
$J=20\frac{1}{2}$	16 783.949	16 731.323	16 716.253	16 713.516	16 627.185	16 612.504
$^2\Pi_{3/2}$	97.29	0.45	0.02	2.11	0.11	0.03
$\kappa\ ^2\Pi_{1/2}$	0.01	75.05	0.11	12.27	0.60	11.96
$^2\Pi_{1/2}$	0.78	2.92	59.57	35.73	0.13	0.87
$\kappa\ ^2\Pi_{3/2}$	1.80	5.67	30.69	39.04	19.40	3.40
$\mu\ ^2\Pi_{3/2}$	0.11	3.00	9.13	10.70	70.16	6.90
$\mu\ ^2\Pi_{1/2}$	0.02	12.92	0.47	0.15	9.60	76.84
$J=40\frac{1}{2}$	17 165.522	17 117.256	17 095.778	17 091.794	17 011.802	16 991.951
$^2\Pi_{3/2}$	95.27	1.06	0.08	3.46	0.07	0.06
$\kappa\ ^2\Pi_{1/2}$	0.04	65.33	6.07	16.48	0.74	11.34
$^2\Pi_{1/2}$	2.55	0.68	49.10	46.60	0.28	0.79
$\kappa\ ^2\Pi_{3/2}$	1.93	13.73	35.19	27.72	14.32	7.12
$\mu\ ^2\Pi_{3/2}$	0.12	7.49	8.28	5.71	65.00	13.40
$\mu\ ^2\Pi_{1/2}$	0.07	11.71	1.29	0.05	19.59	67.28

ide. It is assumed here that the free anion OH^- is a reasonable approximation for the OH^- ligand in the $M^+(OH)^-$ molecule. From velocity modulation laser spectroscopy, Rosenbaum *et al.*[33] have obtained $\omega=3738\ cm^{-1}$ for the harmonic vibration frequency of the ground state of the free OH^- anion. This value will be used as ω_3 in the following calculations for both the $\tilde{X}\ ^2\Sigma^+$ and $\tilde{A}\ ^2\Pi$ states of CaOH. In our previous calculations[6] for the $\tilde{X}$ state, $\omega_3=3600\ cm^{-1}$ was used; this was the value assumed by Lide and Matsumura[18] for alkali hydroxides. We now consider $\omega_3=3738\ cm^{-1}$ is likely a better approximation. Although this assumed value could still contain appreciable error, it was shown in Ref. 6 that the calculations are not sensitive to such error.

For the Ca–O stretch mode, the fundamental frequencies ν_1 were used as approximations of the harmonic frequencies ω_1 for both the $\tilde{A}$ and $\tilde{X}$ states of the two isotopomers. The parameters α_1 in the $\tilde{X}$ state were determined previously[14] from least squares fits of the $B(v_1 00)$ values with $v_1=1-4$ for CaOH and $v_1=1-3$ for CaOD; this was appropriate since the Fermi resonance is J independent and has no effect on the B values in the $\tilde{X}$ state. α_1 for the $\tilde{A}$ state was calculated from $B_v(000)$ and $B_v(100)$. The values of α_3 were taken from the estimates for RbOH and RbOD by Lide and Matsumura[18] for both the $\tilde{A}$ and $\tilde{X}$ states.

The molecular constants, ω_i, α_i, and B_e, for CaOH/CaOD that are used in the following calculations are summarized in Tables VII and VIII for the $\tilde{A}\ ^2\Pi$ and $\tilde{X}\ ^2\Sigma^+$ states, respectively. The two tables also include all the respective results calculated in this section.

Evaluation of equilibrium bond lengths of an $X-Y-Z$ type molecule requires values of the equilibrium moments of inertia for two isotopic molecules, which are expressed by

$$I_e=(m_1m_2r_{12}^2+m_1m_3r_{13}^2+m_2m_3r_{23}^2)/M. \tag{19}$$

Here, $M=m_1+m_2+m_3$, and r_{ij} denote the equilibrium internuclear separations with the labels 1, 2, and 3 corresponding to Ca, O, and H/D atoms, respectively. The moments of inertia, $I_e=h/(8\pi^2cB_e)$, can be calculated directly from the equilibrium rotational constants B_e, defined by

$$B_e=B_v(000)+\tfrac{1}{2}\alpha_1+\tfrac{1}{2}\alpha_3+\alpha_2-\gamma_{22}. \tag{20}$$

There is a γ_{22} term in Eq. (20); this is different from the normal expressions[25] which only include α_i terms. Like α_2, the parameter γ_{22} describes the v_2 dependence of the rotational constant B_v, as shown by Eq. (10). The contribution of the γ_{22} term to B_v is important in CaOH and is dominant, compared with the α_2 term, in CaOD. The values of γ_{22} are listed in Table IV.

Hilborn *et al.*[2] obtained the first estimates of the equilibrium bond lengths based on rotational analysis of the CaOH $\tilde{A}(000)-\tilde{X}(000)$ band and partial analysis of the CaOD $\tilde{A}(000)-\tilde{X}(000)$ band. Now, the values of $B_v(000)$, α_1 and α_2 have been determined from a more precise and much larger data base, including several excited vibrational levels. The results of the present calculations for the $\tilde{A}$ and $\tilde{X}$ states are listed in Tables VII and VIII, respectively.

The results show that while the O–H bond length is essentially the same in the two states, the Ca–O bond length in the $\tilde{A}\,^2\Pi$ state is slightly shorter than that in the $\tilde{X}\,^2\Sigma^+$ state, which indicates that the ''nonbonding'' valence electron is actually slightly antibonding in the $\tilde{X}$ state.

The potential energy function of the CaOH molecule can be expressed in curvilinear internal coordinates in the form,

$$\begin{aligned}V=&\tfrac{1}{2}f_{11}(\Delta r_{12})^2+f_{13}(\Delta r_{12})(\Delta r_{23})+\tfrac{1}{2}f_{33}(\Delta r_{23})^2\\&+\tfrac{1}{2}f_{22}(\Delta\alpha)^2+f_{122}(\Delta r_{12})(\Delta\alpha)^2+f_{322}(\Delta r_{23})(\Delta\alpha)^2\\&+\cdots,\end{aligned} \tag{21}$$

where Δr_{ij} represent the displacements from the equilibrium nuclear separations and $\Delta\alpha$ is the angular displacement associated with the bending vibration. Since the molecular force field expressed in the curvilinear internal expansion is isotopically invariant, it is possible to determine the force field using spectroscopic information from more than one isotopic species. The second property of the force field in these true bond-stretching and angle-bending (curvilinear) coordinates is that the quadratic force field alone gives a good representation of the anharmonicity and, in consequence, the cubic and quartic interaction terms are minimized and the simplest expression for the force field is obtained.[28]

The three harmonic force constants, f_{11}, f_{13}, and f_{33}, may be determined from the harmonic frequencies ω_1 and ω_3 for CaOH, combined with ω_1 for CaOD. The harmonic force constant f_{22} can be calculated from the equilibrium bond lengths and ω_2 of either isotopomer. The methods and equations for such evaluations have been discussed by many authors. The equations employed in this work are referred to Eqs. (22)–(24) in Ref. 6. However, Eq. (24) of Ref. 6, which was obtained from the work of Penny and Sutherland,[34] is in error by a factor of 4, as pointed out previously by Herzberg;[25] the correct equation is

$$f_{22}=4\pi^2c^2\omega_2^2r_{12}^2r_{23}^2\left\{\frac{r_{23}^2}{m_1}+\frac{r_{13}^2}{m_2}+\frac{r_{12}^2}{m_3}\right\}^{-1}. \tag{22}$$

Once f_{11}, f_{13}, and f_{33} were found, the unknown frequency ω_3 for CaOD was calculated from Eqs. (22) and (23) in Ref. 6, and used in further calculations.

For each electronic state ($\tilde{A}$ or $\tilde{X}$), two f_{22} values have been obtained from the two isotopomers and are in excellent agreement, as expected. These values are as follows: $f_{22}(\mathrm{CaOH})=0.0633$ and $f_{22}(\mathrm{CaOD})=0.0647$ mdyn Å for the $\tilde{A}$ state; $f_{22}(\mathrm{CaOH})=0.0605$ and $f_{22}(\mathrm{CaOD})=0.0617$ mdyn Å for the $\tilde{X}$ state. The f_{22} value averaged over the two isotopomers for each state will be used.

The harmonic force constants, f_{11}, f_{13}, f_{33}, and f_{22}, evaluated above are listed in Tables VII and VIII for the $\tilde{A}$ and $\tilde{X}$ states, respectively. As shown in the two tables, the constants f_{11}, f_{33}, and f_{22} in the $\tilde{A}$ state have values that are very close to those in the $\tilde{X}$ state. This is expected since the two states have similar potentials. However, f_{13} has quite different values between the two states. Owing to the large difference in frequency, the coupling between the ν_1 and ν_3 modes is expected to be very weak, and f_{13}, then, has a very small magnitude. It was noticed that f_{13} is sensitive to the uncertainties of the ω_1 values. The uncertainties of f_{13} in the $\tilde{A}$ and $\tilde{X}$ states are probably comparable with the magnitudes of the constants. Thus the f_{13} values are to be considered with caution, while f_{11}, f_{22}, and f_{33} have been determined with confidence.

The Coriolis coupling constants contain valuable information on the harmonic force field. Alternatively, as in the present work, the Coriolis coupling constants can be calculated from the harmonic force field. The values of ζ_{21} and ζ_{23} in the $\tilde{A}$ and $\tilde{X}$ states for both isotopomers, calculated using Eqs. (25) and (26) in Ref. 6, are listed in Tables VII and VIII, respectively.

The l-type doubling constants are dependent on the Coriolis coupling constants and some other constants, ω_1, ω_2, ω_3, and B_e, as expressed by Eq. (15) in Ref. 6. These constants are now available and summarized in Tables VII and VIII. An interesting comparison is possible, therefore, between calculated l-type doubling constants and those determined experimentally. As shown in Table IX(a), it turns out that the calculated q^v values for the $\tilde{A}$ and $\tilde{X}$ states of CaOH and CaOD are all in excellent agreement with the values determined from experimental data. This gives perhaps the most eloquent proof of the quality of the data sets and the deperturbation models in the present work.

Of further interest is a comparison between the experimental centrifugal distortion constants D and those calculated from the derived Coriolis coupling constants and other molecular constants. The expression[35] for D_e is

TABLE VI. Isotope relations of the molecular constants in the $\tilde{A}\ ^2\Pi$ and $\tilde{X}\ ^2\Sigma^+$ states.[a]

	$\tilde{A}\ ^2\Pi$				
	B_v^D/B_v^H	γ_v^D/γ_v^H	A_D^D/A_D^H	p^{e^D}/p^{e^H}	$[q^{e^D}/q^{e^H}]^{1/2}$
(020)	0.910 80(5)			0.914(3)	
(010)	0.908 320(4)	0.946(2)	0.946(10)	0.896(2)	0.93(4)
(100)	0.906 04(1)			0.891(3)	0.88(1)
(000)	0.905 67(2)			0.920(2)	0.93(2)
	$\tilde{X}\ ^2\Sigma^+$				
	B_v^D/B_v^H	γ_v^D/γ_v^H			
(020)	0.911 22(6)				
(010)	0.908 878(6)	0.9493(2)			
(100)	0.906 17(10)				
(000)	0.906 24(2)	0.89(1)			

[a]The superscripts H and D denote CaOH and CaOD, respectively.

$$D_e = 4B_e^3\left\{\frac{\zeta_{23}^2}{\omega_1^2}+\frac{\zeta_{21}^2}{\omega_3^2}\right\}. \tag{23}$$

As shown in Table IX(b), the calculated and experimental values are in remarkably good agreement. This provides further evidence for the quality and self-consistency of the results obtained in the present work.

The vibration–rotation interaction constants α_i provide the main source of information on the cubic anharmonic force field. In the present work only α_2 for the bending vibration will be used for evaluation of the cubic force constants f_{122} and f_{322}. As emphasized earlier, the value of α_2 is very sensitive to isotopic substitution in both $\tilde{A}$ and $\tilde{X}$ states. As expressed in Eq. (10), there are three terms (α_2, γ_{22}, and γ_{ll}) that contribute to $B(0\ \ v_2\ \ 0)$. The parameter α_2 is more than 10 times larger in magnitude than γ_{22} or γ_{ll} for CaOH. However, in CaOD, the parameter α_2 is much smaller than γ_{22} and γ_{ll}; it is essentially zero in both $\tilde{A}$ and $\tilde{X}$ states. This striking isotope effect on the parameter α_2 has also been found in the ground states of CsOH/CsOD and RbOH/RbOD,[18] which also have a linear structure with low frequency bending vibrations. The expression for α_2, given by Eq. (18), contains two cubic force constants, ϕ_{122} and ϕ_{322}, which are the coefficients in the potential function expressed in dimensionless normal coordinates. These two force constants change values upon isotopic substitution and, in consequence, cannot be determined from isotopic information. Lide and Matsumura[18] have performed a coordinate transformation and expressed the parameter α_2 in terms of the cubic force constants, f_{122} and f_{322}, which are the coefficients in the potential in curvilinear internal coordinates. This expression for α_2 also involves the harmonic force constants ($f_{11}, f_{22}, f_{33}, f_{13}$) since the harmonic force field in curvilinear coordinates makes large contributions, upon coordinate transformation, to the anharmonic force constants in the normal coordinates. f_{122} and f_{322} are isotopically invariant. They were then derived using the α_2 values for the two isotopic molecules and many other parameters listed in Tables VII and VIII. Detailed procedures and equations for the derivations are referred to Sec. VI in Ref. 6. The values of f_{122} and f_{322} obtained for the $\tilde{A}$ and $\tilde{X}$ states are listed in Tables VII and VIII, respectively. As seen from the two tables, f_{122} has essentially the same values in the two states. In the process of the calculations, it appeared that this constant, f_{122}, is not very sensitive to the inaccuracy of any individual parameter that was employed in the calculation and, consequently, it has been well determined. On the other hand, the constant f_{322} is very sensitive to inaccuracies of f_{13}. This is probably the major reason for the large difference between the values found for the $\tilde{A}$ and $\tilde{X}$ states. The coupling between the ν_2 and ν_3 modes is believed to be very weak. The uncertainty of the calculated f_{322} is probably quite large and this constant is to be considered with caution. The coefficients of f_{322} in the expression for α_2 are very small compared with those of f_{122} for both isotopomers. Therefore, f_{322} only makes a very small contribution to α_2 and its inaccuracy does not significantly affect the value of f_{122}.

IX. CONCLUSION

The $\tilde{A}\ ^2\Pi(100)/(020)-\tilde{X}\ ^2\Sigma^+(020)/(000)$ bands of CaOD have been rotationally analyzed; the measured line positions form a large and highly precise data base. The corresponding bands of CaOH have been reconsidered with two more subbands and some higher J rotational transitions added to the data set. The global matrix deperturbation reproduces the observed quantities almost to within the experi-

TABLE VII. Molecular parameters[a] for CaOH and CaOD in the $\tilde{A}\ ^2\Pi$ state.

	CaOH	CaOD		CaOH/CaOD
ω_1	628.482	618.776	r_e(Ca–O)	1.9532 Å
ω_2	366.435	278.325	r_e(O–H)	0.9572 Å
ω_3	3738[b]	2709		
B_e	0.343 654 2	0.310 264 3	f_{11}	2.849 mdyn/Å
α_1	0.002 315 3(70)	0.001 970 9(98)	f_{13}	0.908 mdyn/Å
α_2	0.001 164(9)	−0.000 001(13)	f_{33}	7.894 mdyn/Å
α_3	0.000 397[c]	0.000 587[c]	f_{22}	0.0640 mdyn Å
ζ_{21}	0.160 3	0.203 7	f_{122}	−0.167 mdyn
ζ_{23}	0.987 1	0.979 0	f_{322}	0.227 mdyn

[a]ω_i, α_i, and B_e are in unit of cm^{-1}.
[b]Estimated based on Ref. 33.
[c]Estimated values in Ref. 18.

TABLE VIII. Molecular parameters[a] for CaOH and CaOD in the $\tilde{X}\ ^2\Sigma^+$ state.

	CaOH	CaOD		CaOH/CaOD
ω_1	614.79	603.59	r_e(Ca–O)	1.9746 Å
ω_2	357.23	270.71	r_e(O–H)	0.9562 Å
ω_3	3738[b]	2717		
B_e	0.336 613 6	0.304 160 2	f_{11}	2.669 mdyn/Å
α_1	0.002 200(10)	0.001 877(22)	f_{13}	0.463 mdyn/Å
α_2	0.001 093(6)	−0.000 011(12)	f_{33}	7.850 mdyn/Å
α_3	0.000 397[c]	0.000 587[c]	f_{22}	0.0611 mdyn Å
ζ_{21}	0.142 8	0.180 1	f_{122}	−0.165 mdyn
ζ_{23}	0.989 8	0.983 6	f_{322}	0.136 mdyn

[a]ω_i, α_i, and B_e are in unit of cm^{-1}.
[b]Estimated based on Ref. 33.
[c]Estimated values in Ref. 18.

TABLE IX. (a) Calculated and experimental values (cm^{-1}) of q^v. (b) Calculated and experimental values (cm^{-1}) of D.

(a)

	CaOH		CaOD	
	Exp.[a]	Calc.	Exp.[a]	Calc.
$\tilde{A}$	$-0.6978(17)\times10^{-3}$	-0.7031×10^{-3}	$-0.7576(14)\times10^{-3}$	-0.7492×10^{-3}
$\tilde{X}$	$-0.7181(2)\times10^{-3}$	-0.6837×10^{-3}	$-0.7621(4)\times10^{-3}$	-0.7324×10^{-3}

(b)

	CaOH		CaOD	
	Exp.[b]	Calc.	Exp.[b]	Calc.
$\tilde{A}$	$0.3891(11)\times10^{-6}$	0.4008×10^{-6}	$0.2981(15)\times10^{-6}$	0.2997×10^{-6}
$\tilde{X}$	$0.386\,00(3)\times10^{-6}$	0.3957×10^{-6}	$0.2943(16)\times10^{-6}$	0.2994×10^{-6}

[a]Values for the (010) levels.
[b]Values for the (000) levels.

mental uncertainties, in spite of the close degeneracy of some vibronic levels and consequent strong Fermi interactions in the upper state. The fitted molecular constants are consistent with those for the (010) and (000) levels and, in particular, still obey isotope relations quite well.

The Fermi resonance parameters W_1 have been well determined for the $\tilde{A}\ ^2\Pi$ state of both isotopomers. One would normally expect the Fermi resonance parameters to be highly correlated with the zero-order vibrational spacing, $\Delta = T^0(100) - T^0(020)$. Indeed, this is the case in the $\tilde{X}\ ^2\Sigma^+$ electronic state. However, in the $\tilde{A}\ ^2\Pi$ electronic state, the (100) and (020) levels are split into several components due to the spin–orbit and vibronic couplings. Since only one of the two (100) spin components interacts strongly with one or two of the (020) vibronic components, the uneven Fermi interactions within the vibronic manifold break the correlation and lead to unequivocal determinations of W_1, $T^0(100)$, and $T^0(020)$. In addition, the J-independent Fermi resonance matrix elements cause J-dependent interactions because of two factors. The first is the near degeneracy of the interacting vibronic components which have different effective B values. The second is the cross effect of the Fermi resonance operator with the S-uncoupling and/or K-type doubling operators. Fitting such J-dependent interactions certainly helps in determining the Fermi resonance parameters, as well as other parameters.

The vibration–rotation interaction parameters, α_i, are the main source of information on the cubic anharmonic force field. The force constants f_{122} and f_{322} have been derived from the α_2 values of the two isotopic species. The Fermi resonance parameters are another valuable source and have given a direct and accurate measure of the cubic force constant, ϕ_{122}. It would be most desirable if a nonlinear transformation of the coordinate system could be made so that the force constants (f_{ij} and f_{ijj}) in the curvilinear internal coordinates could be converted to the force constants (ϕ_{ij} and ϕ_{ijj}) in the dimensionless normal coordinates and, then, be compared with the results (ϕ_{122}) obtained directly from the experiments (Fermi resonance). Unfortunately, such transformation requires a computer program that was not available to us at the time of this work.

The equilibrium bond lengths, force field and Coriolis coupling constants for the CaOH molecule have been evaluated. The quality of these results has been assessed by calculating the l-type doubling constants q^v and the centrifugal distortion constants D and, then, comparing them with the corresponding values obtained directly from experimental data. The excellent agreement in these comparisons confirms the reliability of the results.

ACKNOWLEDGMENTS

We thank Dr. John Brown for valuable discussions on the Hamiltonian. Support for this work through a research grant from the Natural Sciences and Engineering Research Council of Canada is gratefully acknowledged.

[1] R. F. Wormsbecher, M. Trkula, C. Martner, R. E. Penn, and D. O. Harris, J. Mol. Spectrosc. **97**, 29 (1983).
[2] R. C. Hilborn, Zhu Qingshi, and D. O. Harris, J. Mol. Spectrosc. **97**, 73 (1983).
[3] J. B. West, R. S. Bradford, Jr., J. D. Eversole, and C. R. Jones, Rev. Sci. Instrum. **46**, 164 (1975).
[4] P. F. Bernath and C. R. Brazier, Astrophys. J. **288**, 373 (1985).
[5] M. Li and J. A. Coxon, J. Chem. Phys. **97**, 8961 (1992).
[6] M. Li and J. A. Coxon, J. Chem. Phys. **102**, 2663 (1995).
[7] J. A. Coxon, M. Li, and P. I. Presunka, J. Mol. Spectrosc. **150**, 33 (1991).
[8] D. R. Woodward, D. A. Fletcher, and J. M. Brown, Mol. Phys. **62**, 517 (1987).
[9] E. Fermi, Z. Phys. **71**, 250 (1931).
[10] J. T. Hougen, J. Chem. Phys. **37**, 403 (1962).
[11] T. J. Odiorne and P. R. Brooks, J. Chem. Phys. **55**, 1981 (1971).
[12] A. Gupta, D. S. Perry, and R. N. Zare, J. Chem. Phys. **72**, 6250 (1980).
[13] S. Gerstenkorn and P. Luc, *Atlas du Spectre d'Absorption de la Molécule d'Iode* (Laboratoire Aimé-Cotton, CNRS II—91405 Orsay, France).
[14] J. A. Coxon, M. Li, and P. I. Presunka, Mol. Phys. **76**, 1463 (1992).
[15] M. Li and J. A. Coxon, Can. J. Phys. **72**, 1200 (1994).
[16] J. T. Hougen and J. P. Jesson, J. Chem. Phys. **38**, 1524 (1963).
[17] A. J. Merer and J. M. Allegretti, Can. J. Phys. **49**, 2859 (1971).
[18] D. R. Lide, Jr. and C. Matsumura, J. Chem. Phys. **50**, 3080 (1969).
[19] J. M. Brown (private communication, 1995).
[20] L. M. Ziurys, W. L. Barclay, and M. M. Anderson, Astrophys. J. **384**, L63 (1992).
[21] See AIP document no. PAPS JCPSA-104-4961-18 for 18 pages of tables

of rotational transitions in the $\tilde{A}\,^2\Pi(100)/(020)-\tilde{X}\,^2\Sigma^+(020)/(000)$ bands of CaOH and CaOD. Order by PAPS number and journal reference from American Institute of Physics, Physics Auxiliary Publication Service, Carolyn Gelbach, 500 Sunnyside Boulevard, Woodbury, New York 11797-2999. The price is $1.50 for each microfiche (98 pages) or $5.00 for photocopies of up to 30 pages, and $0.15 for each additional page over 30 pages. Airmail additional. Make checks payable to the American Institute of Physics.

[22] J. M. Brown and F. Jorgensen, Mol. Phys. **47**, 1065 (1982).

[23] J. M. Brown and F. Jorgensen, Adv. Chem. Phys. **52**, 117 (1983).

[24] C. N. Jarman and P. F. Bernath, J. Chem. Phys. **97**, 1711 (1992).

[25] G. Herzberg, *Infrared and Raman Spectra of Polyatomic Molecules* (Van Nostrand, Princeton, 1945).

[26] R. N. Dixon, D. Field, and M. Noble, Chem. Phys. Lett. **50**, 1 (1977).

[27] H. H. Nielsen, Rev. Mod. Phys. **23**, 90 (1951).

[28] I. M. Mills, *Theoretical Chemistry, Specialist Periodical Reports* (The Chemical Society, London, 1974).

[29] D. A. Fletcher, M. A. Anderson, W. L. Barclay, Jr., and L. M. Ziurys, J. Chem. Phys. **102**, 4334 (1995).

[30] J. M. Brown, E. A. Colbourn, J. K. G. Watson, and F. D. Wayne, J. Mol. Spectrosc. **74**, 294 (1979).

[31] L. Veseth, J. Mol. Spectrosc. **38**, 228 (1971).

[32] J. M. Brown and J. K. G. Watson, J. Mol. Spectrosc. **65**, 65 (1977).

[33] N. H. Rosenbaum, J. C. Owrutsky, L. M. Tack, and R. J. Saykally, J. Chem. Phys. **84**, 5308 (1986).

[34] W. G. Penney and G. B. B. M. Sutherland, Proc. R. Soc. London **156**, 654 (1936).

[35] F. Dorman and C. C. Lin, J. Mol. Spectrosc. **12**, 119 (1964).